

## Ranking Causal Anomalies for System Fault Diagnosis via Temporal and Dynamical Analysis on Vanishing Correlations

WEI CHENG<sup>‡</sup>, NEC Laboratories America  
 JINGCHAO NI<sup>‡</sup>, Case Western Reserve University  
 KAI ZHANG, NEC Laboratories America  
 HAIFENG CHEN, NEC Laboratories America  
 GUOFEI JIANG, NEC Laboratories America  
 YU SHI, University of Illinois at Urbana-Champaign  
 XIANG ZHANG, Pennsylvania State University  
 WEI WANG, University of California, Los Angeles

Modern world has witnessed a dramatic increase in our ability to collect, transmit and distribute real-time monitoring and surveillance data from large-scale information systems and cyber-physical systems. Detecting system anomalies thus attracts significant amount of interest in many fields such as security, fault management, and industrial optimization. Recently, invariant network has shown to be a powerful way in characterizing complex system behaviours. In the invariant network, a node represents a system component and an edge indicates a stable, significant interaction between two components. Structures and evolutions of the invariance network, in particular the vanishing correlations, can shed important light on locating causal anomalies and performing diagnosis. However, existing approaches to detect causal anomalies with the invariant network often use the percentage of vanishing correlations to rank possible casual components, which have several limitations: 1) fault propagation in the network is ignored; 2) the root casual anomalies may not always be the nodes with a high-percentage of vanishing correlations; 3) temporal patterns of vanishing correlations are not exploited for robust detection; 4) prior knowledges on anomalous nodes are not exploited for (semi-)supervised detection. To address these limitations, in this paper we propose a network diffusion based framework to identify significant causal anomalies and rank them. Our approach can effectively model fault propagation over the entire invariant network, and can perform joint inference on both the structural, and the time-evolving broken invariance patterns. As a result, it can locate high-confidence anomalies that are truly responsible for the vanishing correlations, and can compensate for unstructured measurement noise in the system. Moreover, when the prior knowledges on the anomalous status of some nodes are available at certain time points, our approach is able to leverage them to further enhance the anomaly inference accuracy. When the prior knowledges are noisy, our approach also automatically learns reliable information and reduces impacts from noises. By performing extensive experiments on synthetic datasets, bank information system datasets, and coal plant cyber-physical system datasets, we demonstrate the effectiveness of our approach.

CCS Concepts: • **Security and privacy** → **Pseudonymity, anonymity and untraceability**;

Additional Key Words and Phrases: causal anomalies ranking, label propagation, nonnegative matrix factorization

---

<sup>‡</sup> These authors contributed equally to this work.

Author's addresses: W. Cheng and Kai Zhang and Haifeng Chen and Guofei Jiang, NEC Laboratories America; Jingchao Ni, Department of Electrical Engineering and Computer Science, Case Western Reserve University; Yu Shi, Department of Computer Science, University of Illinois at Urbana-Champaign; Xiang Zhang, College of Information Sciences and Technology, Pennsylvania State University; Wei Wang, Department of Computer Science, University of California, Los Angeles.

Permission to make digital or hard copies of all or part of this work for personal or classroom use is granted without fee provided that copies are not made or distributed for profit or commercial advantage and that copies bear this notice and the full citation on the first page. Copyrights for components of this work owned by others than ACM must be honored. Abstracting with credit is permitted. To copy otherwise, or republish, to post on servers or to redistribute to lists, requires prior specific permission and/or a fee. Request permissions from [permissions@acm.org](mailto:permissions@acm.org).

© 2016 ACM. 1539-9087/2016/03-ART39 \$15.00

DOI: 0000001.0000001

**ACM Reference Format:**

Wei Cheng, Jingchao Ni, Kai Zhang, Haifeng Chen, Guofei Jiang, Yu Shi, Xiang Zhang, Wei Wang, 2016. Ranking causal anomalies via temporal and dynamical analysis on vanishing correlations *ACM Trans. Embedd. Comput. Syst.* 9, 4, Article 39 (March 2016), 27 pages.  
DOI: 0000001.0000001

**1. INTRODUCTION**

With the rapid advances in networking, computers, and hardware, we are facing an explosive growth of complexity in networked applications and information services. These large-scale, often distributed, information systems usually consist of a great variety of components that work together in a highly complex and coordinated manner. One example is the Cyber-Physical System (CPS) which is typically equipped with a large number of networked sensors that keep recording the running status of the local components; another example is the large scale Information Systems such as the cloud computing facilities in Google, Yahoo! and Amazon, whose composition includes thousands of components that vary from operating systems, application softwares, servers, to storage, networking devices, etc.

A central task in running these large scale distributed systems is to automatically monitor the system status, detect anomalies, and diagnose system fault, so as to guarantee stable and high-quality services or outputs. Significant research efforts have been devoted to this topic in the literatures. For instance, Gertler et al. [Gertler 1998] proposed to detect anomalies by examining monitoring data of individual component with a thresholding scheme. However, it can be quite difficult to learn a universal and reliable threshold in practice, due to the dynamic and complex nature of information systems. More effective and recent approaches typically start with building system profiles, and then detect anomalies via analyzing patterns in these profiles [Chandola et al. 2009; Jiang et al. 2006a]. The system profile is usually extracted from historical time series data collected by monitoring different system components, such as the flow intensity of software log files, the system audit events and the network traffic statistics, and sometimes sensory measurements in physical systems.

The invariant model is a successful example [Jiang et al. 2006a; 2006b] for large-scale system management. It focuses on discovering stable, significant dependencies between pairs of system components that are monitored through time series recordings, so as to profile the system status and perform subsequent reasoning. A strong dependency between a pair of components is called *invariant* (correlation) relationship. By combining the invariants learned from all monitoring components, a global system dependency profile can be obtained. The significant practical value of such an *invariant* profile is that it provides important clues on abnormal system behaviors and in particular the source of anomalies, by checking whether existing invariants are broken. Fig. 1 illustrates one example of the invariant network and two snapshots of broken invariants at time  $t_1$  and  $t_2$ , respectively. Each node represents the observation from a monitoring component. The green line signifies an invariant link between two components, and a red line denotes broken invariant (i.e., vanishing correlation). The network including all the broken invariants at given time point is referred to as the *broken network*.

Although the broken invariants provide valuable information of the system status, how to locate true, causal anomalies can still be a challenging task due to the following reasons. First, system faults are seldom isolated. Instead, starting from the root location/component, anomalous behavior will propagate to neighboring components [Jiang et al. 2006a], and different types of system faults can trigger diverse propagation patterns. Second, monitoring data often contains a lot of noises due to the fluctuation of complex operation environments.

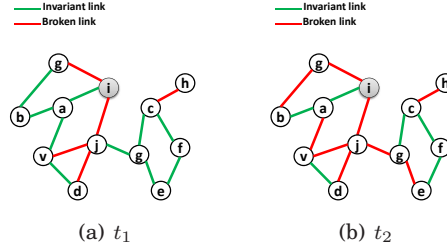


Fig. 1. Invariant network and vanishing correlations (red edges).

Recently, several ranking algorithms were developed to diagnose the system failure based on the percentage of broken invariant edges associated with the nodes, such as the egonet based method proposed by Ge et al. [Ge et al. 2014], and the loopy belief propagation (LBP) based method proposed by Tao et al. [Tao et al. 2014]. Despite the success in practical applications, existing methods still have certain limitations. First, they do not take into account the global structure of the invariant network, neither how the root anomaly/fault propagates in such a network. Second, the ranking strategies rely heavily on the percentage of broken edges connected to a node. For example, the mRank algorithm [Ge et al. 2014] calculated the anomaly score of a given node using the ratio of broken edges within the egonet<sup>1</sup> of the node. The LBP-based method [Tao et al. 2014] used the ratio of broken edges as the prior probability of abnormal state for each node. We argue that, the percentage of broken edges may not serve as a good evidence of the causal anomaly. This is because, although one broken edge can indicate that one (or both) of related nodes is abnormal, lack of a broken edge does not necessary indicate that related nodes are problem free. Instead, it is possible that the correlation is still there when two nodes become abnormal simultaneously [Jiang et al. 2006a]. Therefore the percentage of broken edges could give false evidences. For example, in Fig. 1, the causal anomaly is node ①. The percentage of broken edges for node ① is  $2/3$ , which is smaller than that of node ② (which is equal to 1). Since there exists a clear evidence of fault propagation on node ①, an ideal algorithm should rank ① higher than ②. Third, existing methods usually consider static broken network instead of multiple broken networks at successive time points together. While we believe that, jointly analyzing temporal broken networks can help resolve ambiguity and achieve a denoising effect. This is because, the root casual anomalies usually remain unchanged within a short time period, even though the fault may keep prorogating in the invariant network. As an example shown in Fig. 1, it would be easier to detect the causal anomaly if we jointly consider the broken networks at two successive time points together.

Furthermore, in some applications, system experts may have prior knowledges on the anomalous status of some components (i.e., nodes) at certain time points, such as a numeric value indicating the bias of the monitoring data of a component from its predicted normal values [Chen et al. 2008]. Thus it is highly desirable to incorporate them to guide the causal anomaly inferences. However, to our best knowledge, none of these existing approaches can handle such information.

To address the limitations of existing methods, we propose several network diffusion based algorithms for ranking causal anomalies. Our contributions are summarized as follows.

<sup>1</sup>An egonet is the induced 1-step subgraph for each node.

- (1) We employ the network diffusion process to model propagation of causal anomalies and use propagated anomaly scores to reconstruct the vanishing correlations. By minimizing the reconstruction error, the proposed methods simultaneously consider the whole invariant network structure and the potential fault propagation. We also provide rigid theoretical analysis on the properties of our methods.
- (2) We further develop efficient algorithms which reduce the time complexity from  $\mathcal{O}(n^3)$  to  $\mathcal{O}(n^2)$ , where  $n$  is the number of nodes in the invariant network. This makes it feasible to quickly locate root cause anomalies in large-scale systems.
- (3) We employ effective normalization strategy on the ranking scores, which can reduce the influence of extreme values or outliers without having to explicitly remove them from the data.
- (4) We develop a smoothing algorithm that enables users to jointly consider dynamic and time-evolving broken network, and thus obtain better ranking results.
- (5) We extend our algorithms to semi-supervised settings to leverage the prior knowledges on the anomalous degrees of nodes at certain time points. The prior knowledges are allowed to partially cover the nodes in the invariant network, as practically suggested by the limitation of such information.
- (6) We also improve our semi-supervised algorithms to allow automatic identification of noisy prior knowledges. By assigning small weights to nodes with false anomalous degrees, our algorithms can reduce the negative impacts of prior knowledges and obtain robust performance gain.
- (7) We evaluate the proposed methods on both synthetic datasets and two real-life datasets, including the bank information system and the coal plant cyber-physical system datasets. The experimental results demonstrate the effectiveness of the proposed methods.

## 2. BACKGROUND AND PROBLEM DEFINITION

In this section, we first introduce the technique of the invariant model [Jiang et al. 2006a] and then define our problem.

### 2.1. System Invariant and Vanishing Correlations

The *invariant* model is used to uncover significant pairwise relations among massive set of time series. It is based on the AutoRegressive eXogenous (ARX) model [Lennart 1999] with time delay. Let  $x(t)$  and  $y(t)$  be a pair of time series under consideration, where  $t$  is the time index, and let  $n$  and  $m$  be the degrees of the ARX model, with a delay factor  $k$ . Let  $\hat{y}(t; \theta)$  be the prediction of  $y(t)$  using the ARX model parameterized by  $\theta$ , which can then be written as

$$\hat{y}(t; \theta) = a_1 y(t-1) + \dots + a_n y(t-n) \quad (1)$$

$$+ b_0 x(t-k) + \dots + b_m x(t-k-m) + d$$

$$= \varphi(t)^\top \theta, \quad (2)$$

where  $\theta = [a_1, \dots, a_n, b_0, \dots, b_m, d]^\top \in \mathbb{R}^{n+m+2}$ ,  $\varphi(t) = [y(t-1), \dots, y(t-n), x(t-k), \dots, x(t-k-m), 1]^\top \in \mathbb{R}^{n+m+2}$ . For a given setting of  $(n, m, k)$ , the parameter  $\theta$  can be estimated with observed time points  $t = 1, \dots, N$  in the training data, via least-square fitting. In real-world applications such as anomaly detection in physical systems,  $0 \leq n, m, k \leq 2$  is a popular choice [Chen et al. 2008; Jiang et al. 2006a]. We can define the “goodness of fit” (or *fitness score*) of an ARX model as

$$F(\theta) = 1 - \sqrt{\frac{\sum_{t=1}^N |y(t) - \hat{y}(t; \theta)|^2}{\sum_{t=1}^N |y(t) - \bar{y}|^2}}, \quad (3)$$

Table I. Summary of notations

Symbol	Definition
$n$	the number of nodes in the invariant network
$c, \lambda, \tau$	the parameters $0 < c < 1, \tau > 0, \lambda > 0$
$\sigma(\cdot)$	the softmax function
$\mathcal{G}_l$	the invariant network
$\mathcal{G}_b$	the broken network for $\mathcal{G}_l$
$\mathbf{A} (\tilde{\mathbf{A}}) \in \mathbb{R}^{n \times n}$	the (normalized) adjacency matrix of $\mathcal{G}_l$
$\mathbf{P} (\tilde{\mathbf{P}}) \in \mathbb{R}^{n \times n}$	the (normalized) adjacency matrix of $\mathcal{G}_b$
$\mathbf{M} \in \mathbb{R}^{n \times n}$	the logical matrix of $\mathcal{G}_l$
$d(i)$	the degree of the $i^{th}$ node in network $\mathcal{G}_l$
$\mathbf{D} \in \mathbb{R}^{n \times n}$	the degree matrix: $\mathbf{D} = \text{diag}(d(i), \dots, d(n))$
$\mathbf{r} \in \mathbb{R}^{n \times 1}$	the prorogated anomaly score vector
$\mathbf{e} \in \mathbb{R}^{n \times 1}$	the ranking vector of causal anomalies
RCA	the basic ranking causal anomalies algorithm
R-RCA	the relaxed RCA algorithm
RCA-SOFT	the RCA with softmax normalization
R-RCA-SOFT	the relaxed RCA with softmax normalization
T-RCA	the RCA with temporal smoothing
T-R-RCA	the R-RCA with temporal smoothing
T-RCA-SOFT	the RCA-SOFT with temporal smoothing
T-R-RCA-SOFT	the R-RCA-SOFT with temporal smoothing
RCA-SEMI	the RCA in semi-supervised setting
W-RCA-SEMI	the semi-supervised RCA with weight learning

where  $\bar{y}$  is the mean of the time series  $y(t)$ . A higher value of  $F(\theta)$  indicates a better fitting of the model. An invariant (correlation) is declared on a pair of time series  $x$  and  $y$  if the fitness score of the ARX model is larger than a pre-defined threshold. A network including all the invariant links is referred to as the *invariant network*. Construction of the invariant network is referred to as the model training. The model  $\theta$  will then be applied on the time series  $x$  and  $y$  in the testing phase to track vanishing correlations.

To track vanishing correlations, we can use the techniques developed in [Chen et al. 2008; Jiang et al. 2007]. At each time point, we compute the (normalized) residual  $R(t)$  between the measurement  $y(t)$  and its estimate  $\hat{y}(t; \theta)$  by

$$R(t) = \frac{|y(t) - \hat{y}(t; \theta)|}{\varepsilon_{\max}}, \quad (4)$$

where  $\varepsilon_{\max}$  is the maximum training error  $\varepsilon_{\max} = \max_{1 \leq t \leq N} |y(t) - \hat{y}(t; \theta)|$ . If the residual exceeds a prefixed threshold, then we declare the invariant as “broken”, i.e., the correlation between the two time series vanishes. The network including all the broken edges at given time point and all nodes in the invariant network is referred to as the *broken network*.

## 2.2. Problem Definition

Let  $\mathcal{G}_l$  be the invariant network with  $n$  nodes. Let  $\mathcal{G}_b$  be the broken network for  $\mathcal{G}_l$ . We use two symmetric matrices  $\mathbf{A} \in \mathbb{R}^{n \times n}$ ,  $\mathbf{P} \in \mathbb{R}^{n \times n}$  to denote the adjacency matrix of network  $\mathcal{G}_l$  and  $\mathcal{G}_b$ , respectively. These two matrices can be obtained as discussed in Section 2.1. The two matrices can be binary or continuous. For binary case of  $\mathbf{A}$ , 1 is used to denote that the correlation exists between two time series, and 0 denotes the lack of correlation; while for  $\mathbf{P}$ , 1 is used to denote that the correlation is broken (vanishing), and 0 otherwise. For the continuous case, the fitness score  $F(\theta)$  (3) and the residual  $R(t)$  (4) can be used to fill the two matrices, respectively.

Our main goal is to detect the abnormal nodes in  $\mathcal{G}_l$  that are most responsible for causing the broken edges in  $\mathcal{G}_b$ . In this sense, we call such nodes “causal anomalies”.

Accurate detection of causal anomalous nodes will be extremely useful for examination, debugging and repair of system failures.

### 3. RANKING CAUSAL ANOMALIES

In this section, we present the algorithm of Ranking Causal Anomalies (RCA), which takes into account both the fault propagation and fitting of broken invariants simultaneously.

#### 3.1. Fault Propagation

We consider a very practical scenario of fault propagation, namely anomalous system status can always be traced back to a set of *root cause* anomaly nodes, or *causal anomalies*, as initial seeds. As the time passes, these root cause anomalies will then propagate along the invariant network, most probably towards their neighbors via paths identified by the invariant links in  $\mathcal{G}_l$ . To explicitly model this spreading process on the network, we have employed the label propagation technique [Kim et al. 2008; Tong et al. 2006; Zhou et al. 2004]. Suppose that the (unknown) root cause anomalies are denoted by the indicator vector  $\mathbf{e}$ , whose entries  $e_i$ 's ( $1 \leq i \leq n$ ) indicate whether the  $i$ th node is the causal anomaly ( $e_i = 1$ ) or not ( $e_i = 0$ ). At the end of propagation, the system status is represented by the anomaly score vector  $\mathbf{r}$ , whose entries tell us how severe each node of the network has been impaired. The propagation from  $\mathbf{e}$  to  $\mathbf{r}$  can be modeled by the following optimization problem

$$\min_{\mathbf{r} \geq \mathbf{0}} c \sum_{i,j=1}^n \mathbf{A}_{ij} \left\| \frac{1}{\sqrt{\mathbf{D}_{ii}}} \mathbf{r}_i - \frac{1}{\sqrt{\mathbf{D}_{jj}}} \mathbf{r}_j \right\|^2 + (1-c) \sum_{i=1}^n \|\mathbf{r}_i - \mathbf{e}_i\|^2,$$

where  $\mathbf{D} \in \mathbb{R}^{n \times n}$  is the degree matrix of  $\mathbf{A}$ ,  $c \in (0, 1)$  is the regularization parameter,  $\mathbf{r}$  is the anomaly score vector after the propagation of the initial faults in  $\mathbf{e}$ . We can re-write the above problem as

$$\min_{\mathbf{r} \geq \mathbf{0}} c \mathbf{r}^\top (\mathbf{I}_n - \tilde{\mathbf{A}}) \mathbf{r} + (1-c) \|\mathbf{r} - \mathbf{e}\|_F^2, \quad (5)$$

where  $\mathbf{I}_n$  is the identity matrix,  $\tilde{\mathbf{A}} = \mathbf{D}^{-1/2} \mathbf{A} \mathbf{D}^{-1/2}$  is the degree-normalized version of  $\mathbf{A}$ . Similarly we will use  $\tilde{\mathbf{P}}$  as the degree-normalized  $\mathbf{P}$  in the sequel. The first term in Eq. (5) is the *smoothness constraint* [Zhou et al. 2004], meaning that a good ranking function should assign similar values to nearby nodes in the network. The second term is the *fitting constraint*, which means that the final status should be close to the initial configuration. The trade-off between these two competing constraints is controlled by a positive parameter  $c$ : a small  $c$  encourages a sufficient propagation, and a big  $c$  actually suppresses the propagation. The optimal solution of problem (5) is [Zhou et al. 2004]

$$\mathbf{r} = (1-c)(\mathbf{I}_n - c\tilde{\mathbf{A}})^{-1} \mathbf{e}, \quad (6)$$

which establishes an explicit, closed-form solution between the initial configuration  $\mathbf{e}$  and the final status  $\mathbf{r}$  through propagation.

To encode the information of the broken network, we propose to use  $\mathbf{r}$  to reconstruct the broken network  $\mathcal{G}_b$ . The intuition is illustrated in Fig. 2. If there exists a broken link in  $\mathcal{G}_b$ , e.g.,  $\tilde{\mathbf{P}}_{ij}$  is large, then ideally at least one of the nodes  $i$  and  $j$  should be abnormal, or equivalently, either  $\mathbf{r}_i$  or  $\mathbf{r}_j$  should be large. Thus, we can use the product of  $\mathbf{r}_i$  and  $\mathbf{r}_j$  to reconstruct the value of  $\tilde{\mathbf{P}}_{ij}$ . In Section 5, we'll further discuss how to normalize them to avoid extreme values. Then, the loss of reconstructing the broken link  $\tilde{\mathbf{P}}_{ij}$  can be calculated by  $(\mathbf{r}_i \cdot \mathbf{r}_j - \tilde{\mathbf{P}}_{ij})^2$ . The reconstruction error of the whole broken network is then  $\|(\mathbf{r}\mathbf{r}^\top) \circ \mathbf{M} - \tilde{\mathbf{P}}\|_F^2$ . Here,  $\circ$  is element-wise operator, and  $\mathbf{M}$

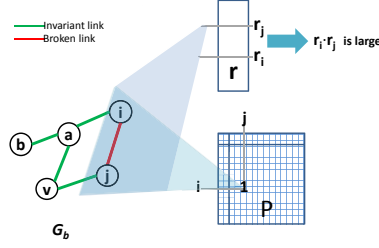


Fig. 2. Reconstruction of the broken invariant network using anomaly score vector  $\mathbf{r}$ .

is the logical matrix of the invariant network  $\mathcal{G}_l$  (1 with edge, 0 without edge). Let  $\mathbf{B} = (1 - c)(\mathbf{I}_n - c\tilde{\mathbf{A}})^{-1}$ , by substituting  $\mathbf{r}$  we obtain the following objective function.

$$\min_{\mathbf{e}_i \in \{0,1\}, 1 \leq i \leq n} \|(\mathbf{B}\mathbf{e}\mathbf{e}^\top \mathbf{B}^\top) \circ \mathbf{M} - \tilde{\mathbf{P}}\|_F^2 \quad (7)$$

Considering that the integer programming in problem (7) is NP-hard, we relax it by using the  $\ell_1$  penalty on  $\mathbf{e}$  with parameter  $\tau$  to control the number of non-zero entries in  $\mathbf{e}$  [Tibshirani 1996]. Then we reach the following objective function.

$$\min_{\mathbf{e} \geq 0} \|(\mathbf{B}\mathbf{e}\mathbf{e}^\top \mathbf{B}^\top) \circ \mathbf{M} - \tilde{\mathbf{P}}\|_F^2 + \tau \|\mathbf{e}\|_1 \quad (8)$$

### 3.2. Learning Algorithm

In this section, we present an iterative multiplicative updating algorithm to optimize the objective function in (8). The objective function is invariant under these updates if and only if  $\mathbf{e}$  are at a stationary point [Lee and Seung 2001]. The solution is presented in the following theorem, which is derived from the Karush-Kuhn-Tucker (KKT) complementarity condition [Boyd and Vandenberghe 2004]. Detailed theoretical analysis of the optimization procedure will be presented in the next section.

**THEOREM 1.** *Updating  $\mathbf{e}$  according to Eq. (9) will monotonically decrease the objective function in Eq. (8) until convergence.*

$$\mathbf{e} \leftarrow \mathbf{e} \circ \left\{ \frac{4\mathbf{B}^\top (\tilde{\mathbf{P}} \circ \mathbf{M})^\top \mathbf{B}\mathbf{e}}{4\mathbf{B}^\top [\mathbf{M} \circ (\mathbf{B}\mathbf{e}\mathbf{e}^\top \mathbf{B}^\top)] \mathbf{B}\mathbf{e} + \tau \mathbf{1}_n} \right\}^{\frac{1}{4}}, \quad (9)$$

where  $\circ$ ,  $\left[ \cdot \right]$  and  $(\cdot)^{\frac{1}{4}}$  are element-wise operators.

Based on Theorem 1, we develop the iterative multiplicative updating algorithm for optimization and summarize it in Alg. 1. We refer to this ranking algorithm as RCA.

### 3.3. Theoretical Analysis

**3.3.1. Derivation.** We derive the solution to problem (9) following the constrained optimization theory [Boyd and Vandenberghe 2004]. Since the objective function is not jointly convex, we adopt an effective multiplicative updating algorithm to find a local optimal solution. We prove Theorem 1 in the following.

**ALGORITHM 1: Ranking Causal Anomalies (RCA)**

**Input:** Network  $\mathcal{G}_l$  denoting the invariant network with  $n$  nodes, and is represented by an adjacency matrix  $\mathbf{A}$ ,  $c$  is the network propagation parameter,  $\tau$  is the parameter to control the sparsity of  $\mathbf{e}$ ,  $\tilde{\mathbf{P}}$  is the normalized adjacency matrix of the broken network,  $\mathbf{M}$  is the logical matrix of  $\mathcal{G}_l$  (1 with edge, 0 without edge)

**Output:** Ranking vector  $\mathbf{e}$

```

1 begin
2   for  $i \leftarrow 1$  to  $n$  do
3      $\mathbf{D}_{ii} \leftarrow \sum_{j=1}^n \mathbf{A}_{ij}$ ;
4   end
5    $\mathbf{D} \leftarrow \text{diag}(\mathbf{D}_{11}, \dots, \mathbf{D}_{nn})$ ;
6    $\tilde{\mathbf{A}} \leftarrow \mathbf{D}^{-1/2} \mathbf{A} \mathbf{D}^{-1/2}$ ;
7   Initialize  $\mathbf{e}$  with random values between (0,1];
8    $\mathbf{B} \leftarrow (1 - c)(\mathbf{I}_n - c\tilde{\mathbf{A}})^{-1}$ ;
9   repeat
10    | Update  $\mathbf{e}$  by Eq. (9);
11  until convergence;
12 end

```

We formulate the Lagrange function for optimization  $L = \|(\mathbf{B}\mathbf{e}\mathbf{e}^\top \mathbf{B}^\top) \circ \mathbf{M} - \tilde{\mathbf{P}}\|_F^2 + \tau \mathbf{1}_n^\top \mathbf{e}$ . Obviously,  $\mathbf{B}$ ,  $\mathbf{M}$  and  $\tilde{\mathbf{P}}$  are symmetric matrix. Let  $\mathbf{F} = (\mathbf{B}\mathbf{e}\mathbf{e}^\top \mathbf{B}^\top) \circ \mathbf{M}$ , then

$$\begin{aligned}
\frac{\partial}{\partial \mathbf{e}_m} (\mathbf{F} - \tilde{\mathbf{P}})_{ij}^2 &= 2(\mathbf{F}_{ij} - \tilde{\mathbf{P}}_{ij}) \frac{\partial \mathbf{F}_{ij}}{\partial \mathbf{e}_m} \\
&= 4(\mathbf{F}_{ij} - \tilde{\mathbf{P}}_{ij}) \mathbf{M}_{ij} (\mathbf{B}_{mi}^\top \mathbf{B}_j \mathbf{e}) \quad (\text{by symmetry}) \\
&= 4\mathbf{B}_{mi}^\top (\mathbf{F}_{ij} - \tilde{\mathbf{P}}_{ij}) \mathbf{M}_{ij} (\mathbf{B}\mathbf{e})_j.
\end{aligned} \tag{10}$$

It follows that

$$\frac{\partial \|\mathbf{F} - \tilde{\mathbf{P}}\|_F^2}{\partial \mathbf{e}_m} = 4\mathbf{B}_{mi}^\top [(\mathbf{F} - \tilde{\mathbf{P}}) \circ \mathbf{M}] (\mathbf{B}\mathbf{e}), \tag{11}$$

and thereby

$$\frac{\partial \|\mathbf{F} - \tilde{\mathbf{P}}\|_F^2}{\partial \mathbf{e}} = 4\mathbf{B}^\top [(\mathbf{F} - \tilde{\mathbf{P}}) \circ \mathbf{M}] (\mathbf{B}\mathbf{e}). \tag{12}$$

Thus, the partial derivative of Lagrange function with respect to  $\mathbf{e}$  is:

$$\nabla_{\mathbf{e}} L = 4\mathbf{B}^\top [(\mathbf{B}\mathbf{e}\mathbf{e}^\top \mathbf{B}^\top - \tilde{\mathbf{P}}) \circ \mathbf{M}] \mathbf{B}\mathbf{e} + \tau \mathbf{1}_n, \tag{13}$$

where  $\mathbf{1}_n$  is the  $n \times 1$  vector of all ones. Using the Karush-Kuhn-Tucker (KKT) complementarity condition [Boyd and Vandenberghe 2004] for the non-negative constraint on  $\mathbf{e}$ , we have

$$\nabla_{\mathbf{e}} L \circ \mathbf{e} = \mathbf{0} \tag{14}$$

The above formula leads to the updating rule for  $\mathbf{e}$  that is shown in Eq. (9).

**3.3.2. Convergence.** We use the auxiliary function approach [Lee and Seung 2001] to prove the convergence of Eq. (9) in Theorem 1. We first introduce the definition of auxiliary function as follows.

**DEFINITION 3.1.**  $Z(h, \hat{h})$  is an auxiliary function for  $L(h)$  if the conditions

$$Z(h, \hat{h}) \geq L(h) \quad \text{and} \quad Z(h, h) = L(h), \tag{15}$$



are satisfied for any given  $h, \hat{h}$  [Lee and Seung 2001].

**LEMMA 3.1.** *If  $Z$  is an auxiliary function for  $L$ , then  $L$  is non-increasing under the update [Lee and Seung 2001].*

$$h^{(t+1)} = \underset{h}{\operatorname{argmin}} Z(h, h^{(t)}) \quad (16)$$

**THEOREM 2.** *Let  $L(\mathbf{e})$  denote the sum of all terms in  $L$  containing  $\mathbf{e}$ . The following function*

$$\begin{aligned} Z(\mathbf{e}, \hat{\mathbf{e}}) = & -2 \sum_{ij} \left[ \mathbf{B}^\top (\tilde{\mathbf{P}} \circ \mathbf{M})^\top \mathbf{B} \right]_{ij} \hat{\mathbf{e}}_i \hat{\mathbf{e}}_j \left( 1 + \log \frac{\mathbf{e}_i \mathbf{e}_j}{\hat{\mathbf{e}}_i \hat{\mathbf{e}}_j} \right) \\ & + \sum_i \left\{ \mathbf{B}^\top [\mathbf{M} \circ (\mathbf{B} \hat{\mathbf{e}} \hat{\mathbf{e}}^\top \mathbf{B}^\top)] \mathbf{B} \hat{\mathbf{e}} \right\}_i \frac{\mathbf{e}_i^4}{\hat{\mathbf{e}}_i^3} + \frac{\tau}{4} \sum_i \frac{\mathbf{e}_i^4 + 3\hat{\mathbf{e}}_i^4}{\hat{\mathbf{e}}_i^3} \end{aligned} \quad (17)$$

is an auxiliary function for  $L(\mathbf{e})$ . Furthermore, it is a convex function in  $\mathbf{e}$  and has a global minimum.

**PROOF.** According to Definition 3.1, in this proof, we need to verify (1)  $Z(\mathbf{e}, \hat{\mathbf{e}}) \geq L(\mathbf{e})$ , (2)  $Z(\mathbf{e}, \mathbf{e}) = L(\mathbf{e})$  and (3)  $Z(\mathbf{e}, \hat{\mathbf{e}})$  is a convex function in  $\mathbf{e}$ , which are respectively proved as following.

First, omitting some constants, we write  $L(\mathbf{e})$  as

$$L(\mathbf{e}) = -2\operatorname{tr} \left( \mathbf{B}^\top (\tilde{\mathbf{P}} \circ \mathbf{M})^\top \mathbf{B} \mathbf{e} \mathbf{e}^\top \right) + \operatorname{tr} \left( [\mathbf{M} \circ (\mathbf{B} \mathbf{e} \mathbf{e}^\top \mathbf{B}^\top)]^\top (\mathbf{B} \mathbf{e} \mathbf{e}^\top \mathbf{B}^\top) \right) + \tau \sum_i \mathbf{e}_i \quad (18)$$

In order to prove (1)  $Z(\mathbf{e}, \hat{\mathbf{e}}) \geq L(\mathbf{e})$ , we deduce the upper bound for each term in Eq. (18).

Using the inequality  $z \geq 1 + \log z$ , which holds for any  $z > 0$ , we have

$$\frac{\mathbf{e}_i \mathbf{e}_j}{\hat{\mathbf{e}}_i \hat{\mathbf{e}}_j} \geq 1 + \log \frac{\mathbf{e}_i \mathbf{e}_j}{\hat{\mathbf{e}}_i \hat{\mathbf{e}}_j}$$

Then we can write an upper bound for the first term

$$\begin{aligned} -2\operatorname{tr} \left( \mathbf{B}^\top (\tilde{\mathbf{P}} \circ \mathbf{M})^\top \mathbf{B} \mathbf{e} \mathbf{e}^\top \right) &= -2 \sum_{ij} \left[ \mathbf{B}^\top (\tilde{\mathbf{P}} \circ \mathbf{M})^\top \mathbf{B} \right]_{ij} \mathbf{e}_i \mathbf{e}_j \\ &\leq -2 \sum_{ij} \left[ \mathbf{B}^\top (\tilde{\mathbf{P}} \circ \mathbf{M})^\top \mathbf{B} \right]_{ij} \hat{\mathbf{e}}_i \hat{\mathbf{e}}_j \left( 1 + \log \frac{\mathbf{e}_i \mathbf{e}_j}{\hat{\mathbf{e}}_i \hat{\mathbf{e}}_j} \right) \end{aligned} \quad (19)$$

For the second term, we can rewrite it by

$$\operatorname{tr} \left( [\mathbf{M} \circ (\mathbf{B} \mathbf{e} \mathbf{e}^\top \mathbf{B}^\top)]^\top (\mathbf{B} \mathbf{e} \mathbf{e}^\top \mathbf{B}^\top) \right) = \sum_{xyijpq} \mathbf{M}_{xy} \mathbf{B}_{xi} \mathbf{e}_i \mathbf{e}_j \mathbf{B}_{yj} \mathbf{B}_{xp} \mathbf{e}_p \mathbf{e}_q \mathbf{B}_{yq}$$

Let  $\mathbf{e}_i = \hat{\mathbf{e}}_i s_i$ ,  $\mathbf{e}_j = \hat{\mathbf{e}}_j s_j$ ,  $\mathbf{e}_p = \hat{\mathbf{e}}_p s_p$  and  $\mathbf{e}_q = \hat{\mathbf{e}}_q s_q$  for some non-negative values  $s_i$ ,  $s_j$ ,  $s_p$  and  $s_q$ , we can further rewrite it by

$$\begin{aligned} & \sum_{xyijpq} \mathbf{M}_{xy} \mathbf{B}_{xi} \hat{\mathbf{e}}_i \hat{\mathbf{e}}_j \mathbf{B}_{yj} \mathbf{B}_{xp} \hat{\mathbf{e}}_p \hat{\mathbf{e}}_q \mathbf{B}_{yq} s_i s_j s_p s_q \\ & \leq \sum_{xyijpq} \mathbf{M}_{xy} \mathbf{B}_{xi} \hat{\mathbf{e}}_i \hat{\mathbf{e}}_j \mathbf{B}_{yj} \mathbf{B}_{xp} \hat{\mathbf{e}}_p \hat{\mathbf{e}}_q \mathbf{B}_{yq} \frac{s_i^4 + s_j^4 + s_p^4 + s_q^4}{4} \\ & = \frac{1}{4} \left( \sum_i \mathbf{Q}_i \frac{\mathbf{e}_i^4}{\hat{\mathbf{e}}_i^3} + \sum_j \mathbf{Q}_j \frac{\mathbf{e}_j^4}{\hat{\mathbf{e}}_j^3} + \sum_p \mathbf{Q}_p \frac{\mathbf{e}_p^4}{\hat{\mathbf{e}}_p^3} + \sum_q \mathbf{Q}_q \frac{\mathbf{e}_q^4}{\hat{\mathbf{e}}_q^3} \right) = \sum_i \mathbf{Q}_i \frac{\mathbf{e}_i^4}{\hat{\mathbf{e}}_i^3} \end{aligned} \quad (20)$$

where  $\mathbf{Q} = \mathbf{B}^\top [\mathbf{M} \circ (\mathbf{B} \hat{\mathbf{e}} \hat{\mathbf{e}}^\top \mathbf{B}^\top)] \mathbf{B} \hat{\mathbf{e}}$ . Here, the last equation is obtained by switching indexes.

For the third term, using the fact that  $2ab \leq a^2 + b^2$ , we have

$$\tau \sum_i \mathbf{e}_i \leq \frac{\tau}{2} \sum_i \frac{\mathbf{e}_i^2 + \hat{\mathbf{e}}_i^2}{\hat{\mathbf{e}}_i} \leq \frac{\tau}{4} \sum_i \frac{\mathbf{e}_i^4 + 3\hat{\mathbf{e}}_i^4}{\hat{\mathbf{e}}_i^3} \quad (21)$$

Therefore, by collecting Eq. (19), Eq. (20) and Eq. (21), we have verified (1)  $Z(\mathbf{e}, \hat{\mathbf{e}}) \geq L(\mathbf{e})$ . Moreover, by substituting  $\hat{\mathbf{e}}$  with  $\mathbf{e}$  in  $Z(\mathbf{e}, \hat{\mathbf{e}})$ , we can directly verify (2)  $Z(\mathbf{e}, \mathbf{e}) = L(\mathbf{e})$ .

To prove (3)  $Z(\mathbf{e}, \hat{\mathbf{e}})$  is a convex function in  $\mathbf{e}$ , we need to show the Hessian matrix  $\nabla_{\mathbf{e}}^2 Z(\mathbf{e}, \hat{\mathbf{e}})$  is positive-definite. First, we derive

$$\frac{\partial Z(\mathbf{e}, \hat{\mathbf{e}})}{\partial \mathbf{e}_i} = -4 \left[ \mathbf{B}^\top (\tilde{\mathbf{P}} \circ \mathbf{M})^\top \mathbf{B} \hat{\mathbf{e}} \right]_i \frac{\hat{\mathbf{e}}_i}{\mathbf{e}_i} + 4 \left\{ \mathbf{B}^\top [\mathbf{M} \circ (\mathbf{B} \hat{\mathbf{e}} \hat{\mathbf{e}}^\top \mathbf{B}^\top)] \mathbf{B} \hat{\mathbf{e}} \right\}_i \frac{\mathbf{e}_i^3}{\hat{\mathbf{e}}_i^3} + \tau \frac{\mathbf{e}_i^3}{\hat{\mathbf{e}}_i^3}$$

Then the second order derivative is

$$\frac{\partial^2 Z(\mathbf{e}, \hat{\mathbf{e}})}{\partial \mathbf{e}_i \partial \mathbf{e}_j} = \delta_{ij} \left( 4 \left[ \mathbf{B}^\top (\tilde{\mathbf{P}} \circ \mathbf{M})^\top \mathbf{B} \hat{\mathbf{e}} \right]_i \frac{\hat{\mathbf{e}}_i}{\mathbf{e}_i^2} + 12 \left\{ \mathbf{B}^\top [\mathbf{M} \circ (\mathbf{B} \hat{\mathbf{e}} \hat{\mathbf{e}}^\top \mathbf{B}^\top)] \mathbf{B} \hat{\mathbf{e}} \right\}_i \frac{\mathbf{e}_i^2}{\hat{\mathbf{e}}_i^3} + 3\tau \frac{\mathbf{e}_i^2}{\hat{\mathbf{e}}_i^3} \right)$$

where  $\delta_{ij}$  is the Kronecker delta.  $\delta_{ij} = 1$  if  $i = j$ ;  $\delta_{ij} = 0$  otherwise.

Therefore, the Hessian matrix  $\nabla_{\mathbf{e}}^2 Z(\mathbf{e}, \hat{\mathbf{e}})$  is a diagonal matrix with positive diagonal entries. Hence, we verify (3)  $\nabla_{\mathbf{e}}^2 Z(\mathbf{e}, \hat{\mathbf{e}})$  is positive-definite and  $Z(\mathbf{e}, \hat{\mathbf{e}})$  is a convex function in  $\mathbf{e}$ . This completes the proof.  $\square$

Based on Theorem 2, we can minimize  $Z(\mathbf{e}, \hat{\mathbf{e}})$  with respect to  $\mathbf{e}$  with  $\hat{\mathbf{e}}$  fixed. We set  $\nabla_{\mathbf{e}} Z(\mathbf{e}, \hat{\mathbf{e}}) = \mathbf{0}$ , and get the following updating formula

$$\mathbf{e} \leftarrow \hat{\mathbf{e}} \circ \left\{ \frac{4\mathbf{B}^\top (\tilde{\mathbf{P}} \circ \mathbf{M})^\top \mathbf{B} \hat{\mathbf{e}}}{4\mathbf{B}^\top [\mathbf{M} \circ (\mathbf{B} \hat{\mathbf{e}} \hat{\mathbf{e}}^\top \mathbf{B}^\top)] \mathbf{B} \hat{\mathbf{e}} + \tau \mathbf{1}_n} \right\}^{\frac{1}{4}}, \quad (22)$$

which is consistent with the updating formula derived from the KKT condition aforementioned.

From Lemma 3.1 and Theorem 2, for each subsequent iteration of updating  $\mathbf{e}$ , we have  $L(\mathbf{e}^0) = Z(\mathbf{e}^0, \mathbf{e}^0) \geq Z(\mathbf{e}^1, \mathbf{e}^0) \geq Z(\mathbf{e}^1, \mathbf{e}^1) = L(\mathbf{e}^1) \geq \dots \geq L(\mathbf{e}^{Iter})$ . Thus  $L(\mathbf{e})$  monotonically decreases. Since the objective function Eq. (8) is lower bounded by 0, the correctness of Theorem 1 is proven.

**3.3.3. Complexity Analysis.** In Algorithm 1, we need to calculate the inverse of an  $n \times n$  matrix, which takes  $\mathcal{O}(n^3)$  time. In each iteration, the multiplication between two  $n \times n$  matrices is inevitable, thus the overall time complexity of Algorithm 1 is  $\mathcal{O}(Iter \cdot n^3)$ ,

where  $Iter$  is the number of iterations needed for convergence. In the following section, we will propose an efficient algorithm that reduces the time complexity to  $\mathcal{O}(Iter \cdot n^2)$ .

#### 4. COMPUTATIONAL SPEED UP

In this section, we will propose an efficient algorithm that avoids the matrix inverse calculations as well as the multiplication between two  $n \times n$  matrices. The time complexity can be reduced to  $\mathcal{O}(Iter \cdot n^2)$ .

We achieve the computational speed up by relaxing the objective function in (8) to jointly optimize  $\mathbf{r}$  and  $\mathbf{e}$ . The objective function is shown in the following.

$$\min_{\mathbf{e} \geq \mathbf{0}, \mathbf{r} \geq \mathbf{0}} \underbrace{c\mathbf{r}^\top (\mathbf{I}_n - \tilde{\mathbf{A}})\mathbf{r} + (1-c)\|\mathbf{r} - \mathbf{e}\|_F^2}_{\text{Fault propagation}} + \underbrace{\lambda\|(\mathbf{r}\mathbf{r}^\top) \circ \mathbf{M} - \tilde{\mathbf{P}}\|_F^2 + \tau\|\mathbf{e}\|_1}_{\text{Vanishing correlation reconstruction}} \quad (23)$$

To optimize this objective function, we can use an alternating scheme. That is, we optimize the objective with respect to  $\mathbf{r}$  while fixing  $\mathbf{e}$ , and vice versa. This procedure continues until convergence. The objective function is invariant under these updates if and only if  $\mathbf{r}, \mathbf{e}$  are at a stationary point [Lee and Seung 2001]. Specifically, the solution to the optimization problem in Eq. (23) is based on the following theorem, which is derived from the Karush-Kuhn-Tucker (KKT) complementarity condition [Boyd and Vandenberghe 2004]. The derivation of it and the proof of Theorem 3 is similar to that of Theorem 1.

**THEOREM 3.** *Alternatively updating  $\mathbf{e}$  and  $\mathbf{r}$  according to Eq. (24) and Eq. (25) will monotonically decrease the objective function in Eq. (23) until convergence.*

$$\mathbf{r} \leftarrow \mathbf{r} \circ \left\{ \frac{\tilde{\mathbf{A}}\mathbf{r} + 2\lambda(\tilde{\mathbf{P}} \circ \mathbf{M})\mathbf{r} + (1-c)\mathbf{e}}{\mathbf{r} + 2\lambda[(\mathbf{r}\mathbf{r}^\top) \circ \mathbf{M}]\mathbf{r}} \right\}^{\frac{1}{4}} \quad (24)$$

$$\mathbf{e} \leftarrow \mathbf{e} \circ \left[ \frac{2(1-c)\mathbf{r}}{\tau\mathbf{1}_n + 2(1-c)\mathbf{e}} \right]^{\frac{1}{2}} \quad (25)$$

Based on Theorem 3, we can develop the iterative multiplicative updating algorithm for optimization similar to Algorithm 1. Due to page limit we skip the details. We refer to this ranking algorithm as R-RCA. From Eq. (24) and Eq. (25), we observe that the calculation of the inverse of the  $n \times n$  matrix and the multiplication between two  $n \times n$  matrices in Algorithm 1 are not necessary. As we will see in Section 8.5, the relaxed versions of our algorithm can greatly improve the computational efficiency.

#### 5. SOFTMAX NORMALIZATION

In Section 3, we use the product  $\mathbf{r}_i \cdot \mathbf{r}_j$  as the strength of evidence that the correlation between node  $i$  and  $j$  is vanishing (broken). However, it suffers from the extreme values in the ranking values  $\mathbf{r}$ . To reduce the influence of the extreme values or outliers, we employ the softmax normalization on the ranking values  $\mathbf{r}$ . The ranking values are nonlinearly transformed using the sigmoidal function before the multiplication is performed. Thus, the reconstruction error is expressed by  $\|(\sigma(\mathbf{r})\sigma^\top(\mathbf{r})) \circ \mathbf{M} - \tilde{\mathbf{P}}\|_F^2$ , where  $\sigma(\cdot)$  is the softmax function with:

$$\sigma(\mathbf{r})_i = \frac{e^{\mathbf{r}_i}}{\sum_{k=1}^n e^{\mathbf{r}_k}}, (i = 1, \dots, n). \quad (26)$$

The corresponding objective function in Alg. 1 is modified to the following

$$\min_{\mathbf{e} \geq \mathbf{0}} \|(\sigma(\mathbf{B}\mathbf{e})\sigma^\top(\mathbf{B}\mathbf{e})) \circ \mathbf{M} - \tilde{\mathbf{P}}\|_F^2 + \tau\|\mathbf{e}\|_1. \quad (27)$$

Similarly, the objective function for Eq. (23) is modified to the following

$$\min_{\mathbf{e} \geq \mathbf{0}, \mathbf{r} \geq \mathbf{0}} c \mathbf{r}^\top (\mathbf{I}_n - \tilde{\mathbf{A}}) \mathbf{r} + (1 - c) \|\mathbf{r} - \mathbf{e}\|_F^2 + \lambda \|(\sigma(\mathbf{r}) \sigma^\top(\mathbf{r})) \circ \mathbf{M} - \tilde{\mathbf{P}}\|_F^2 + \tau \|\mathbf{e}\|_1. \quad (28)$$

The optimization of these two objective functions are based on the following two theorems.

**THEOREM 4.** *Updating  $\mathbf{e}$  according to Eq. (29) will monotonically decrease the objective function in Eq. (27) until convergence.*

$$\mathbf{e} \leftarrow \mathbf{e} \circ \left\{ \frac{4\mathbf{B}^\top \Psi (\tilde{\mathbf{P}} \circ \mathbf{M}) \sigma(\mathbf{B}\mathbf{e})}{4[\mathbf{B}^\top (\Psi \sigma(\mathbf{B}\mathbf{e}) \sigma^\top(\mathbf{B}\mathbf{e})) \circ \mathbf{M}] \sigma(\mathbf{B}\mathbf{e}) + \tau \mathbf{1}_n} \right\}^{\frac{1}{4}}, \quad (29)$$

where  $\Psi = \{\text{diag}[\sigma(\mathbf{B}\mathbf{e})] - \sigma(\mathbf{B}\mathbf{e}) \sigma^\top(\mathbf{B}\mathbf{e})\}$ .

**THEOREM 5.** *Updating  $\mathbf{r}$  according to Eq. (30) will monotonically decrease the objective function in Eq. (28) until convergence.*

$$\mathbf{r} \leftarrow \mathbf{r} \circ \left\{ \frac{\tilde{\mathbf{A}} \mathbf{r} + 2\lambda \left[ \left( (\sigma(\mathbf{r}) \mathbf{1}_n^\top) \circ \tilde{\mathbf{P}} + \rho \Lambda \right) \circ \mathbf{M} \right] \sigma(\mathbf{r}) + (1 - c) \mathbf{e}}{\mathbf{r} + 2\lambda \left[ \left( (\sigma(\mathbf{r}) \circ \sigma(\mathbf{r})) \sigma^\top(\mathbf{r}) + \sigma(\mathbf{r}) (\sigma^\top(\mathbf{r}) \tilde{\mathbf{P}}) \right) \circ \mathbf{M} \right] \sigma(\mathbf{r})} \right\}^{\frac{1}{4}}, \quad (30)$$

where  $\Lambda = \sigma(\mathbf{r}) \sigma^\top(\mathbf{r})$  and  $\rho = \sigma^\top(\mathbf{r}) \sigma(\mathbf{r})$ .

Theorem 4 and Theorem 5 can be proven with a similar strategy to that of Theorem 1. We refer to the ranking algorithms with *softmax* normalization (Eq. (27) and Eq. (28)) as RCA-SOFT and R-RCA-SOFT respectively.

## 6. TEMPORAL SMOOTHING ON MULTIPLE BROKEN NETWORKS

As discussed in Section 1, although the number of anomaly nodes could increase due to fault propagation in the network, the root cause anomalies will be stable within a short time period  $T$  [Jiang et al. 2006b]. Based on this intuition, we further develop a smoothing strategy by jointly considering the temporal broken networks. Specifically, we add a smoothing term  $\|\mathbf{e}^{(t)} - \mathbf{e}^{(t-1)}\|_2^2$  to the objective functions. Here,  $\mathbf{e}^{(t-1)}$  and  $\mathbf{e}^{(t)}$  are causal anomaly ranking vectors for two successive time points. For example, the objective function of algorithm RCA with temporal broken networks smoothing is shown in Eq. (31).

$$\min_{\mathbf{e}^{(t)} \geq \mathbf{0}, 1 \leq t \leq T} \sum_{t=1}^T \left[ \left\| (\mathbf{B}\mathbf{e}^{(t)} (\mathbf{e}^{(t)})^\top \mathbf{B}^\top) \circ \mathbf{M} - \tilde{\mathbf{P}}^{(t)} \right\|_F^2 + \tau \|\mathbf{e}^{(t)}\|_1 \right] + \underbrace{\alpha \|\mathbf{e}^{(t)} - \mathbf{e}^{(t-1)}\|_2^2}_{\text{Temporal smoothing}} \quad (31)$$

Here,  $\tilde{\mathbf{P}}^{(t)}$  is the degree-normalized adjacency matrix of broken network at time point  $t$ . Similar to the discussion in Section 3.3, we can derive the updating formula of Eq. (31) in the following.

$$\mathbf{e}^{(t)} \leftarrow \mathbf{e}^{(t)} \circ \left\{ \frac{4\mathbf{B}^\top (\tilde{\mathbf{P}}^{(t)} \circ \mathbf{M})^\top \mathbf{B}\mathbf{e}^{(t)} + 2\alpha \mathbf{e}^{(t-1)}}{4\mathbf{B}^\top [\mathbf{M} \circ (\mathbf{B}\mathbf{e}^{(t)} (\mathbf{e}^{(t)})^\top \mathbf{B}^\top)] \mathbf{B}\mathbf{e}^{(t)} + \tau \mathbf{1}_n + 2\alpha \mathbf{e}^{(t)}} \right\}^{\frac{1}{4}} \quad (32)$$

The updating formula for R-RCA, RCA-SOFT, and R-RCA-SOFT with temporal broken networks smoothing is similar. Due to space limit, we skip the details. We refer to the ranking algorithms with temporal networks smoothing as T-RCA, T-R-RCA, T-RCA-SOFT and T-R-RCA-SOFT respectively.

## 7. LEVERAGING PRIOR KNOWLEDGE

In real-life applications, we may have prior knowledges that reflect to what extent a node is harmed by the causal anomalies at a certain time point. In this section, we extend our RCA model to a semi-supervised setting to incorporate such prior knowledge so that the performance of causal anomaly inference can be further enhanced.

### 7.1. Leveraging Node Attributes

One common type of prior knowledge can be represented by a numeric attribute for each node that measures the degree that node is anomalous at the observation time point. For example, the attribute value can be the absolute bias of the monitoring data of a node that deviates from its predicted normal value at a time point [Chen et al. 2008].

Let  $v_i \geq 0$  represent the anomalous degree of node  $i$ , our goal is to leverage these attributes in a principled manner to improve the causal anomaly inference capability of our model. It is important to note that, usually the attributes only partially covers the nodes in the invariant network due to the short of prior knowledges. That is, let  $\mathcal{V}$  be the set of all nodes in the invariant network, then  $v_i$  is only available for node  $i \in \mathcal{V}_p$ , where  $\mathcal{V}_p \subseteq \mathcal{V}$ . To account for this sparsity of prior knowledge, we define an indicator  $u_i \in \{0, 1\}$  for each node  $i$  s.t.  $u_i = 1$  if node  $i$  has a valid  $v_i$ ;  $u_i = 0$  otherwise.

Because  $v_i$  measures the degree that node  $i$  is impacted by causal anomalies, we can use  $r_i$  in Eq. (6) to approximate  $v_i$ . Specifically, we want to minimize the inconsistency of  $u_i(r_i - v_i)^2$ . Let  $\mathbf{v} \in \mathbb{R}_+^{n \times 1}$  with the  $i^{\text{th}}$  entry as  $v_i$  (note  $v_i = 0$  if  $i \notin \mathcal{V}_p$ ), and  $\mathbf{D}_u \in \{0, 1\}^{n \times n}$  be a diagonal matrix with  $(\mathbf{D}_u)_{ii}$  as  $u_i$ , then we can obtain a matrix form of the inconsistencies as  $(\mathbf{r} - \mathbf{v})^\top \mathbf{D}_u (\mathbf{r} - \mathbf{v})$ . By integrating this loss function with our RCA model in Eq. (6), and replacing  $\mathbf{r}$  by  $\mathbf{B}\mathbf{e}$ , we obtain an objective function that enables node attributes as following.

$$\min_{\mathbf{e} \geq 0} \|(\mathbf{B}\mathbf{e}^\top \mathbf{B}^\top) \circ \mathbf{M} - \tilde{\mathbf{P}}\|_F^2 + \tau \|\mathbf{e}\|_1 + \underbrace{\beta (\mathbf{B}\mathbf{e} - \mathbf{v})^\top \mathbf{D}_u (\mathbf{B}\mathbf{e} - \mathbf{v})}_{\text{Leveraging prior knowledge}} \quad (33)$$

where  $\beta$  is a parameter that measures the importance of prior knowledge. Intuitively, the more reliable the prior knowledge, the larger the value of  $\beta$ .

The objective function in Eq. (33) can be optimized by an updating formula as summarized by the following theorem. The derivation of this formula follows a similar strategy as those discussed in Sec. 3.3

**THEOREM 6.** *Updating  $\mathbf{e}$  according to Eq. (34) will monotonically decrease the objective function in Eq. (33) until convergence.*

$$\mathbf{e} \leftarrow \mathbf{e} \circ \left\{ \frac{4\mathbf{B}^\top (\tilde{\mathbf{P}} \circ \mathbf{M})^\top \mathbf{B}\mathbf{e} + 2\beta \mathbf{B}^\top (\mathbf{u} \circ \mathbf{v})}{4\mathbf{B}^\top [\mathbf{M} \circ (\mathbf{B}\mathbf{e}^\top \mathbf{B}^\top)] \mathbf{B}\mathbf{e} + 2\beta \mathbf{B}^\top [\mathbf{u} \circ (\mathbf{B}\mathbf{e})] + \tau \mathbf{1}_n} \right\}^{\frac{1}{4}} \quad (34)$$

The formal algorithm that considers node attributes can be similarly formulated as Alg. 1. In the following, we refer to the semi-supervised ranking algorithm using Eq. (34) as RCA-SEMI.

### 7.2. Learning the Reliability of Prior Knowledge

In real practice, because of noises, not all node attributes are reliable. It is likely that a considerable part of  $\{v_i\}$  is inconsistent with the current broken status of the invariant network and can mislead causal anomaly inference if we trust them without differentiation. To avoid the problem caused by noisy node attributes, next, we develop

a strategy to automatically select reliable node attributes from unreliable ones to improve the robustness of our model.

In Eq. (33), all valid node attributes  $\mathbf{v}_i$  are treated equally by assigning the same weights  $\mathbf{u}_i = 1$ . A more practical design is to allow  $\mathbf{u}_i$  to vary based on the reliability of  $\mathbf{v}_i$ . Ideally,  $\mathbf{u}_i$  is small if  $\mathbf{v}_i$  is inconsistent with the anomalous status of node  $i$  as inferred from fault propagation. This inconsistency can be measured by  $(\mathbf{r}_i - \mathbf{v}_i)^2$ . Therefore, we can modify the optimization problem in Eq. (33) as following to allow automatic learning of  $\mathbf{u}$ .

$$\begin{aligned} \min_{\mathbf{e}, \mathbf{u} \geq \mathbf{0}} \quad & \|(\mathbf{B}\mathbf{e}\mathbf{e}^\top \mathbf{B}^\top) \circ \mathbf{M} - \tilde{\mathbf{P}}\|_F^2 + \tau \|\mathbf{e}\|_1 + \beta \sum_{i \in \mathcal{V}_P} \mathbf{u}_i (\mathbf{B}\mathbf{e} - \mathbf{v})_i^2 + \gamma \sum_{i \in \mathcal{V}_p} \mathbf{u}_i^2 \\ \text{s.t.} \quad & \sum_{i \in \mathcal{V}_p} \mathbf{u}_i = |\mathcal{V}_p| \end{aligned} \quad (35)$$

In the above equation, we enforce the equality constraint to allow different  $\mathbf{u}_i$  to be correlated and comparable for selection purpose. The  $\ell_2$  norm on  $\mathbf{u}$  is enforced to avoid trivial solutions. Without it, all entries in  $\mathbf{u}$  will be zeros except for  $\mathbf{u}_i$  corresponding to the least inconsistency  $(\mathbf{B}\mathbf{e} - \mathbf{v})_i^2$ . Here,  $\gamma$  is a parameter controlling the complexity of  $\mathbf{u}$ . Typically, larger  $\gamma$  results in more non-zero entries in  $\mathbf{u}$ .

Because the problem in Eq. (35) is not jointly convex in  $\mathbf{e}$  and  $\mathbf{u}$ , we take an alternating minimization approach. The solution to the subproblem w.r.t.  $\mathbf{e}$  is the same as Eq. (34). Next, we discuss the solution to  $\mathbf{u}$ .

First, we denote  $\hat{\mathbf{u}} = \mathbf{u}(\mathcal{V}_p)$  to be the projection of  $\mathbf{u}$  on node set  $\mathcal{V}_p$ , and  $\hat{n} = |\mathcal{V}_p|$ . Let  $\mathbf{w} \in \mathbb{R}_+^{\hat{n} \times 1}$  with  $\mathbf{w}_i = (\mathbf{B}\mathbf{e} - \mathbf{v})_i^2$  for  $i \in \mathcal{V}_p$ . Then we can write the subproblem w.r.t.  $\hat{\mathbf{u}}$  as

$$\begin{aligned} \min_{\hat{\mathbf{u}} \geq \mathbf{0}} \quad & \beta \hat{\mathbf{u}}^\top \mathbf{w} + \gamma \hat{\mathbf{u}}^\top \hat{\mathbf{u}} \\ \text{s.t.} \quad & \hat{\mathbf{u}}^\top \mathbf{1}_{\hat{n}} = \hat{n} \end{aligned} \quad (36)$$

where  $\mathbf{1}_{\hat{n}}$  is a length- $\hat{n}$  vector with all entries as 1.

Eq. (36) is a quadratic optimization problem with respect to  $\mathbf{u}$ , whose Lagrangian function can be formulated as following.

$$\mathcal{L}_u(\hat{\mathbf{u}}, \boldsymbol{\eta}, \theta) = \beta \hat{\mathbf{u}}^\top \mathbf{w} + \gamma \hat{\mathbf{u}}^\top \hat{\mathbf{u}} - \hat{\mathbf{u}}^\top \boldsymbol{\eta} - \theta(\hat{\mathbf{u}}^\top \mathbf{1}_{\hat{n}} - \hat{n}) \quad (37)$$

where  $\boldsymbol{\eta} = [\eta_1, \eta_2, \dots, \eta_{\hat{n}}]^\top \geq \mathbf{0}$  and  $\theta \geq 0$  are the Lagrangian multipliers. The optimal  $\hat{\mathbf{u}}^*$  should satisfy the following Karush-Kuhn-Tucker (KKT) conditions [Boyd and Vandenberghe 2004]:

- (1) Stationary condition.  $\nabla_{\hat{\mathbf{u}}^*} \mathcal{L}_u(\hat{\mathbf{u}}, \boldsymbol{\eta}, \theta) = \beta \mathbf{w} + 2\gamma \hat{\mathbf{u}}^* - \boldsymbol{\eta} - \theta \mathbf{1}_{\hat{n}} = \mathbf{0}_{\hat{n}}$
- (2) Feasibility condition.  $\hat{\mathbf{u}}^* \geq \mathbf{0}_{\hat{n}}, (\hat{\mathbf{u}}^*)^\top \mathbf{1}_{\hat{n}} - \hat{n} = 0$
- (3) Complementary slackness.  $\boldsymbol{\eta}_i \hat{\mathbf{u}}_i^* = 0, 1 \leq i \leq \hat{n}$
- (4) Nonnegativity condition.  $\boldsymbol{\eta} \geq \mathbf{0}_{\hat{n}}$

From the stationary condition, we can obtain  $\hat{\mathbf{u}}_i$  as

$$\hat{\mathbf{u}}_i = \frac{\boldsymbol{\eta}_i + \theta - \mathbf{w}_i}{2\gamma}$$

where we can observe that  $\hat{\mathbf{u}}_i$  depends on the specification of  $\boldsymbol{\eta}_i$  and  $\theta$ . Similar to [Yu et al. 2013], we divide the problem into three cases:

- (1) When  $\theta - \mathbf{w}_i > 0$ , since  $\boldsymbol{\eta}_i \geq 0$ , we have  $\hat{\mathbf{u}}_i > 0$ . From the complementary slackness,  $\boldsymbol{\eta}_i \hat{\mathbf{u}}_i = 0$ , we have  $\boldsymbol{\eta}_i = 0$ , therefore,  $\hat{\mathbf{u}}_i = \frac{\theta - \mathbf{w}_i}{2\gamma}$ .
- (2) When  $\theta - \mathbf{w}_i < 0$ , since  $\hat{\mathbf{u}}_i \geq 0$ , we have  $\boldsymbol{\eta}_i > 0$ . Because  $\boldsymbol{\eta}_i \hat{\mathbf{u}}_i = 0$ , we have  $\hat{\mathbf{u}}_i = 0$ .

(3) When  $\theta - w_i = 0$ , we have  $\hat{u}_i = \frac{\eta_i}{2\gamma}$ . Since  $\eta_i \hat{u}_i = 0$ , we have  $\hat{u}_i = 0$  and  $\eta_i = 0$ .

Therefore, if we sort  $w_1 \leq w_2 \leq \dots \leq w_{\hat{n}}$ , there exists  $\tilde{\theta} > 0$  s.t.  $\tilde{\theta} - w_t > 0$  and  $\tilde{\theta} - w_t \leq 0$ . Then  $\hat{u}_i$  can be solved as following.

$$\hat{u}_i = \begin{cases} \frac{\theta - w_i}{2\gamma}, & \text{if } i \leq t \\ 0, & \text{otherwise} \end{cases} \quad (38)$$

where  $\theta$  can be solved by using  $\sum_{i=1}^t \hat{u}_i = \hat{n}$ , i.e.,

$$\theta = \frac{2\gamma\hat{n} + \sum_{i=1}^t w_i}{t} \quad (39)$$

Eq. (38) implies the intuition of the assignment of  $u_i$ . That is, when  $w_i$  is large,  $u_i$  is small. Recall  $w_i$  represents the inconsistency between propagation score  $r_i$  and node attribute  $v_i$ , which may come from the noises in the prior knowledge. Therefore, Eq. (38) assigns small weights to large inconsistencies to reduce the negative impacts of noisy node attributes and get a consensus result, hence improve the robustness of our model.

In Eq. (39),  $\gamma$  relates to the selectivity of the model. When  $\gamma$  is very large,  $\hat{u}_i$  becomes large, and all node attributes will be selected with nearly equal weights. When  $\gamma$  is very small, at least one node attribute (with the smallest  $w_i$ ) will be selected. Therefore, we can use  $\gamma$  to control how many node attributes will be integrated for causal anomaly ranking.

From Eq. (38) and Eq. (39), we can search the value of  $t$  from  $\hat{n}$  to 1 decreasingly [Yu et al. 2013]. Once  $\theta - w_t > 0$ , then we find the value of  $t$ . Then we can calculate  $\hat{u}_1, \dots, \hat{u}_{\hat{n}}$  according to Eq. (38). The algorithm for solving  $u$  is involved in Alg. 2. In Alg. 2,  $e$  and  $u$  are optimized alternately. Since both optimization procedures decrease the value of the objective function in Eq. (35) and the objective function value is lower bounded by 0, Alg. 2 is guaranteed to converge to a local minima of the optimization problem in Eq. (35). In the following, we refer to the semi-supervised ranking algorithm with weight learning as W-RCA-SEMI.

## 8. EMPIRICAL STUDY

In this section, we perform extensive experiments to evaluate the performance of the proposed methods (summarized in Table I). We use both simulated data and real-world monitoring datasets. For comparison, we select several state-of-the-art methods, including mRank and gRank in [Ge et al. 2014; Jiang et al. 2006a], and LBP [Tao et al. 2014]. For all the methods, the tuning parameters were tuned using cross validation. We use several evaluation metrics including precision, recall, and nDCG [Järvelin and Kekäläinen 2002] to measure the performance. The precision and recall are computed on the top- $K$  ranking result, where  $K$  is typically chosen as twice the actual number of ground-truth causal anomalies [Järvelin and Kekäläinen 2002; Tao et al. 2014]. The nDCG of the top- $p$  ranking result is defined as  $nDCG_p = \frac{DCG_p}{IDCG_p}$ , where  $DCG_p = \sum_{i=1}^p \frac{2^{rel_i-1}}{\log_2(1+i)}$ ,  $IDCG_p$  is the  $DCG_p$  value on the ground-truth, and  $p$  is smaller than or equal to the actual number of ground-truth anomalies. The  $rel_i$  represents the anomaly score of the  $i$ th item in the ranking list of the ground-truth.

### 8.1. Simulation Study

We first evaluate the performance of the proposed methods using simulations. We have followed [Ge et al. 2014; Tao et al. 2014] in generating the simulation data.

**ALGORITHM 2: W-RCA-SEMI**

**Input:** Network  $\mathcal{G}_l$  denoting the invariant network with  $n$  nodes, and is represented by an adjacency matrix  $\mathbf{A}$ ,  $c$  is the network propagation parameter,  $\tau$  is the parameter to control the sparsity of  $\mathbf{e}$ ,  $\tilde{\mathbf{P}}$  is the normalized adjacency matrix of the broken network,  $\mathbf{M}$  is the logical matrix of  $\mathcal{G}_l$  (1 with edge, 0 without edge),  $\mathbf{v}$  is the vector of node attributes,  $\mathcal{V}_p$  is the set of nodes having valid node attributes,  $\beta$  is a parameter to control semi-supervision,  $\gamma$  is a parameter to control the complexity of the learned weights

**Output:** Ranking vector  $\mathbf{e}$ , weight vector  $\mathbf{u}$

```

1 begin
2   Initialize  $\hat{\mathbf{u}}_i = 1, \forall i \in \mathcal{V}_p$ ;
3   repeat
4     Set  $\mathbf{u}_i = \hat{\mathbf{u}}_i \forall i \in \mathcal{V}_p; \mathbf{u}_i = 0 \forall i \notin \mathcal{V}_p$ ;
5     Inferring  $\mathbf{e}$  by Eq. (34);
6     Compute  $\mathbf{w}_i = ((\mathbf{B}\mathbf{e})_i - \mathbf{v}_i)^2, \forall i \in \mathcal{V}_p$ ;
7     Sort  $\{\mathbf{w}_i\}_{1 \leq i \leq \hat{n}}$  in increasing order;
8      $t \leftarrow \hat{n} + 1$ ;
9     do
10       $t \leftarrow t - 1$ ;
11       $\theta \leftarrow \frac{2\gamma\hat{n} + \sum_{i=1}^t \mathbf{w}_i}{t}$ ;
12      while  $\theta - \mathbf{w}_t \leq 0$  and  $t > 1$ ;
13      for  $i \leftarrow 1$  to  $t$  do
14         $\hat{\mathbf{u}}_i \leftarrow \frac{\theta - \mathbf{w}_i}{2\gamma}$ ;
15      end
16      for  $i \leftarrow t + 1$  to  $\hat{n}$  do
17         $\hat{\mathbf{u}}_i \leftarrow 0$ ;
18      end
19    until convergence;
20 end

```

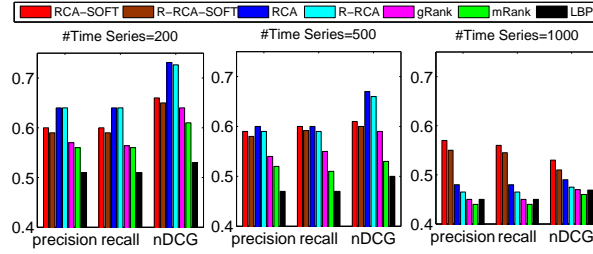
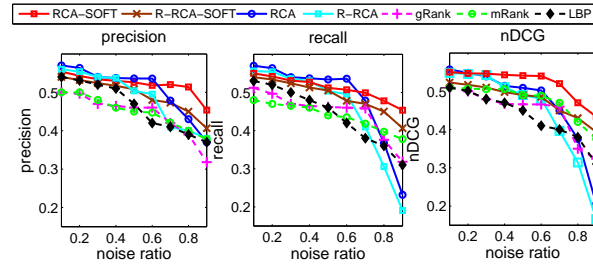
*8.1.1. Data Generation.* We first generate 5000 synthetic time series data to simulate the monitoring records<sup>2</sup>. Each time series contains 1,050 time points. Based on the invariant model introduced in Sec. 2.1, we build the invariant network by using the first 1,000 time points in the time series. This generates an invariant network containing 1,551 nodes and 157,371 edges. To generate invariant network of different sizes, we randomly sample 200, 500, and 1000 nodes from the whole invariant network and evaluate the algorithms on these sub-networks.

To generate the root cause anomaly, we randomly select 10 nodes from the network, and assign each of them an anomaly score between 1 and 10. The ranking of these scores is used as the ground-truth. To simulate the anomaly prorogation, we further use these scores as the vector  $\mathbf{e}$  in Eq. (6) and calculate  $\mathbf{r}$  ( $c = 0.9$ ). The values of the top-30 time series with largest values in  $\mathbf{r}$  are then modified by changing their amplitude value with the ratio  $1 + r_i$ . That is, if the observed values of one time series is  $y_1$ , after changing it from  $y_1$  to  $y_2$ , the manually-injected degree of anomaly  $\frac{|y_2 - y_1|}{|y_1|}$  is equal to  $1 + r_i$ . We denote this anomaly generation scheme as *amplitude-based* anomaly generation.

*8.1.2. Performance Evaluation.* Using the simulated data, we compare the performance of different algorithms. In this example, we only consider the training time series as

<sup>2</sup><http://cs.unc.edu/~weicheng/synthetics5000.csv>




 Fig. 3. Comparison on synthetic data( $K, p = 10$ ).

 Fig. 4. Performance with different noise ratio( $K, p = 10$ ).

one snapshot; multiple snapshot cases involving temporal smoothing will be examined in the real datasets. Due to the page limit, we report the precision, recall and nDCG for only the top-10 items considering that the ground-truth contains 10 anomalies. Similar results can be observed with other settings of  $K$  and  $p$ . For each algorithm, reported result is averaged over 100 randomly selected subsets of the training data.

From Fig. 3, we have several key observations. First, the proposed algorithms significantly outperform other competing methods, which demonstrates the advantage of taking into account fault prorogation in ranking casual anomalies. We also notice that performance of all ranking algorithms will decline on larger invariant networks with more nodes, indicating that anomaly ranking becomes more challenging on networks with more complex behaviour. However, the ranking result with *softmax* is less sensitive to the size of the invariant network, suggesting that the *softmax* normalization can effectively improve the robustness of the algorithm. This is quite beneficial in real-life applications, especially when data are noisy. Finally, we observe that RCA and RCA-SOFT outperform R-RCA and R-RCA-SOFT, respectively. This implies that the relaxed versions of the algorithms are less accurate. Nevertheless, their accuracies are still very comparable to those of the RCA and RCA-SOFT methods. In addition, the efficiency of the relaxed algorithms is greatly improved, as discussed in Sec. 4 and Sec. 8.5.

**8.1.3. Robustness Evaluation.** Practical invariant network and broken edges can be quite noisy. In this section, we further examine the performance of the proposed algorithms w.r.t. different noise levels. To do this, we randomly perturb a portion of non-broken edges in the invariant network. Results are shown in Fig. 4. We observe that, even when the noise ratio approaches 50%, the precision, recall and nDCG of the proposed approaches still attain 0.5. This indicates the robustness of the proposed algorithms. We also observe that, when the noise ratio is very large, RCA-SOFT and R-RCA-SOFT work better than RCA and R-RCA, respectively. This is similar to those

Table II. Examples of categories and monitors.

Categories	Samples of Measurements
CPU	utilization, user usage time, IO wait time
DISK	# of write operations, write time, weighted IO time
MEM	run queue, collision rate, UsageRate
NET	error rate, packet rate
SYS	UTIL, MODE UTIL

Table III. Data set description.

Data Set	#Monitors	#invariant links	#broken edges at given time point
BIS	1273	39116	18052
Coal Plant	1625	9451	56

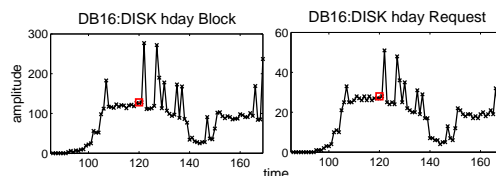


Fig. 5. Two example monitoring data of BIS.

observations made in Sec. 8.1.2. As has been discussed in Sec. 5, the *softmax* normalization can greatly suppress the impact of extreme values and outliers in  $r$ , thus improves the robustness.

## 8.2. Ranking Causal Anomalies on Bank Information System Data

In this section, we apply the proposed methods to detect causal abnormal components on a Bank Information System (BIS) data set [Ge et al. 2014; Tao et al. 2014]. The monitoring data are collected from a real-world bank information system logs, which contain 11 categories. Each category has a varying number of time series, and Table II gives five categories as examples. The data set contains the flow intensities collected every 6 seconds. In total, we have 1,273 flow intensity time series. The training data is collected at normal system states, where each time series has 168 time points. The invariant network is then generated on the training data as described in Sec. 2.1. The testing data of the 1,273 flow intensity time series are collected during abnormal system states, where each time series contain 169 time points. We track the changes of the invariant network with the testing data using the method described in Sec. 2.1. Once we obtain the broken networks at different time points, we will then perform causal anomaly ranking in these temporal slots jointly. Properties of the networks constructed are summarized in Table III.

Based on the knowledge from system experts, the root cause anomaly at  $t = 120$  in the testing data is related to “DB16”. An illustration of two “DB16” related monitoring data are shown in Fig. 5. We highlight  $t = 120$  with red square. Obviously, their behaviour looks anomalous from that time point on. Due to the complex dependency among different monitoring time series (measurements), it is impractical to obtain a full ranking of abnormal measurement. Fortunately, we have a unique semantic label associated with each measurement. For example, some semantic labels read “DB16:DISK hdx Request” and “WEB26 PAGEOUT RATE”. Thus, we can extract all measurements whose titles have the prefix “DB16” as the ground-truth anomalies. The ranking score is determined by the number of broken edges associated with each measurement. Here our goal is to demonstrate how the top-ranked measurements selected by our method are related to the “DB16” root cause. Altogether, there are 80

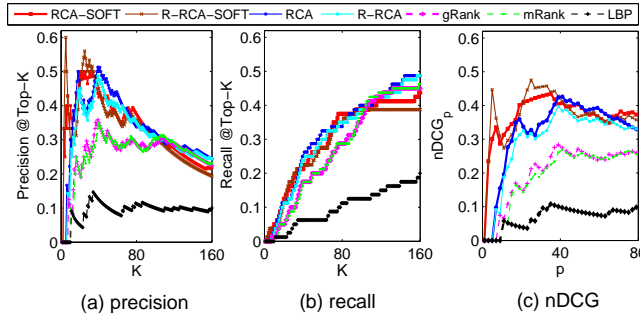


Fig. 6. Comparison on BIS data.

 Table IV. Top 12 anomalies detected by different methods on BIS data( $t:120$ ).

mRank	gRank	LBP	RCA	RCA-SOFT	R-RCA	R-RCA-SOFT
WEB16:NET eth1 BYNETIF	HUB18:MEM UsageRate	WEB22:SYS MODE UTIL	HUB17:DISK hda Request	DB17:DISK hdm Block	HUB17:DISK hda Request	DB17:DISK hdm Block
HUB17:DISK hda Request	HUB17:DISK hda Request	DB15:DISK hdax Block	DB17:DISK hdax Block	DB17:DISK hdax Block	DB15:PACKET Output	DB17:DISK hdax Block
AP12:DISK hd45 Block	AP12:DISK hd45 Block	WEB12:NET eth1 BYNETIF	HUB17:DISK hda Busy	DB16:DISK hdm Block	HUB17:DISK hda Busy	DB16:DISK hdm Block
AP12:DISK hd1 Block	AP12:DISK hd1 Block	WEB17:DISK BYDISK	DB18:DISK hdax Block	DB18:DISK hdm Block	DB17:DISK hdm Block	DB16:DISK hdj Request
WEB19:DISK BYDISK	AP11:DISK hd45 Block	DB18:DISK hdt Busy	DB18:DISK hdm Block	DB16:DISK hdj Request	DB17:DISK hdax Block	DB16:DISK hdax Request
AP11:DISK hd45 Block	AP11:DISK hd1 Block	DB15:DISK hdl Request	DB16:DISK hdm Block	DB18:DISK hdax Block	DB18:DISK hdm Block	DB18:DISK hdag Request
AP11:DISK hd1 Block	DB17:DISK hdax Block	WEB21:DISK BYDISK	DB17:DISK hdax Block	DB16:DISK hdax Request	DB16:DISK hdm Block	DB18:DISK hdm Block
DB16:DISK hdm Block	DB15:PACKET Input	WEB27:FREE UTIL	DB17:DISK hdm Block	DB18:DISK hdag Request	DB18:DISK hdax Block	DB18:DISK hdax Request
DB17:DISK hdm Block	DB17:DISK hdm Block	WEB19:NET eth0	DB16:DISK hdax Block	DB18:DISK hdax Request	DB17:DISK hdax Block	DB18:DISK hdax Request
DB18:DISK hdm Block	DB16:DISK hdm Block	WEB25:PACKET OUT RATE	DB16:DISK hdj Request	DB16:DISK hdax Block	DB16:DISK hdax Block	DB18:DISK hdax Request
DB17:DISK hdax Block	DB17:DISK hdax Block	DB16:DISK hdj Block	DB18:DISK hdag Request	DB18:DISK hda Request	DB16:DISK hdj Request	DB18:DISK hdax Block
DB18:DISK hdax Block	DB18:DISK hdm Block	AP13:DISK hd30 Block	DB16:DISK hdax Request	DB18:DISK hda Request	DB18:DISK hdag Request	DB16:DISK hdj Request

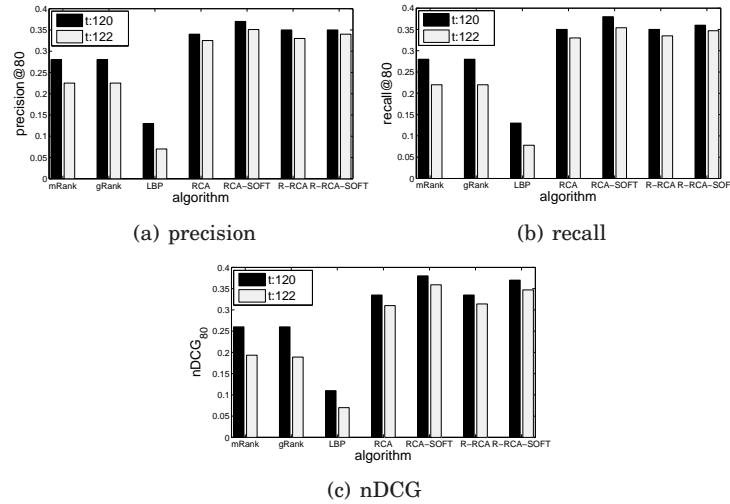
 Table V. Number of “DB16” related monitors in top 32 results on BIS data( $t:120$ ).

mRank	gRank	LBP	RCA	RCA-SOFT	R-RCA	R-RCA-SOFT
10	7	4	14	16	13	17

measurements related to “DB16”, so we report the precision, recall with  $K$  ranging from 1 to 160 and the nDCG with  $p$  ranging from 1 to 80.

The results are shown in Fig. 6. The relative performance of different approaches is consistent with the observations in the simulation study. Again, the proposed algorithms outperform baseline methods by a large margin. To examine the top-ranked items more clearly, we list the top-12 results of different approaches in Table IV and report the number of “DB16”-related monitors in Table V. From Table IV, we observe that the three baseline methods only report one “DB16” related measurement in the top-12 results, and the actual rank of the “DB16”-related measurement appear lower (worse) than that of the proposed methods. We also notice that the ranking algorithms with *softmax* normalization outperform others. From Tables IV and V, we can see that top ranked items reported by RCA-SOFT and R-RCA-SOFT are more relevant than those reported by RCA and R-RCA, respectively. This clearly illustrates the effectiveness of the *softmax* normalization in reducing the influence of extreme values or outliers in the data.

As discussed in Sec. 1, the root anomalies could further propagate from one component to related ones over time, which may or may not necessarily relate to “DB16”. Such anomaly propagation makes anomaly detection even harder. To study how the performance varies at different time points, we compare the performance at  $t = 120$  and  $t = 122$ , respectively in Fig. 7 ( $p, K=80$ ). Clearly, the performance declines for all methods. However, the proposed methods are less sensitive to anomaly propagation than others, suggesting that our approaches can better handle the fault propagation problem. We believe this is attributed to the network diffusion model that explicitly captures the fault propagation processes. We also list the top-12 abnormal at  $t = 122$  in Table VI. Due to page limit, we only show the results of mRank, gRank, RCA-SOFT and R-RCA-SOFT. By comparing the results in Tables IV and VI, we can observe that

Fig. 7. Performance at  $t:120$  v.s.  $t:122$  on BIS data( $p, K=80$ ).Table VI. Top 12 anomalies on BIS data( $t:122$ ).

mRank	gRank	RCA-SOFT	R-RCA-SOFT
WEB21:NET eth1 BYNETIF	WEB21:NET eth0 BYNETIF	DB17:DISK hdm Block	DB17:DISK hdm Block
WEB21:NET eth0 BYNETIF	WEB21:NET eth1 BYNETIF	DB17:DISK hdba Block	DB17:DISK hdba Block
WEB21:FREE UTIL	HUB18:MEM UsageRate	DB16:DISK hdm Block	DB16:DISK hdm Block
AP12:DISK hd45 Block	WEB21:FREE UTIL	DB18:DISK hdm Block	DB16:DISK hdj Request
AP12:DISK hd1 Block	WEB26:PAGEOUT RATE	DB16:DISK hdj Request	DB16:DISK hdax Request
DB18:DISK hday Block	AP12:DISK hd45 Block	DB18:DISK hdba Block	DB18:DISK hdm Block
DB18:DISK hdk Block	AP12:DISK hd1 Block	DB16:DISK hdax Request	DB18:DISK hdx Request
DB18:DISK hday Request	DB18:DISK hday Block	DB16:DISK hdba Block	DB18:DISK hdba Block
DB18:DISK hdk Request	DB18:DISK hdk Block	DB18:DISK hdx Request	DB16:DISK hdba Block
WEB26:PAGEOUT RATE	DB18:DISK hday Request	DB18:DISK hdbl Request	DB18:DISK hdax Request
DB17:DISK hdm Block	DB18:DISK hdk Request	DB16:DISK hdx Busy	DB16:PACKET Inputx
DB16:DISK hdm Block	AP11:DISK hd45 Block	DB16:DISK hdx Request	DB18:DISK hdbl Request

Table VII. Top 12 anomalies reported by methods with temporal smoothing on BIS data( $t:120-121$ ).

T-RCA	T-RCA-SOFT	T-R-RCA	T-R-RCA-SOFT
WEB14:NET eth0 BYNETIF	DB17:DISK hdm Block	WEB14:NET eth0 BYNETIF	DB17:DISK hdm Block
WEB16:DISK BYDSK	DB17:DISK hdba Block	WEB21:NET eth0 BYNETIF	DB17:DISK hdba Block
DB18:DISK hdba Block	DB16:DISK hdm Block	WEB16:DISK BYDSK PHYS	DB16:DISK hdm Block
DB18:DISK hdm Block	DB18:DISK hdm Block	WEB21:FREE UTIL	DB18:DISK hdm Block
DB17:DISK hdba Block	DB16:DISK hdj Request	DB15:PACKET Output	DB16:DISK hdj Request
DB16:DISK hdm Block	DB18:DISK hdba Block	DB16:DISK hdj Request	DB18:DISK hdba Block
DB17:DISK hdm Block	DB16:DISK hdax Request	DB17:DISK hdm Block	DB16:DISK hdax Request
DB16:DISK hdba Block	DB16:DISK hdba Block	DB16:DISK hdba Block	DB18:DISK hdx Request
DB16:DISK hdj Request	DB18:DISK hdx Request	DB17:DISK hday Block	DB16:DISK hdba Block
DB16:DISK hdax Request	DB18:DISK hdbl Request	DB16:DISK hdm Block	DB18:DISK hdbl Request
DB16:DISK hdx Busy	DB16:DISK hdx Busy	DB16:DISK hdax Request	DB16:DISK hdx Request
DB16:DISK hdbl Busy	DB16:DISK hdx Request	DB18:DISK hdba Block	DB16:DISK hdx Busy

Table VIII. Comparison on the number of “DB16” related anomalies in top-12 results on BIS data.

	RCA	RCA-SOFT	R-RCA	R-RCA-SOFT
<b>Without temporal smoothing</b>	4	4	3	4
<b>With temporal smoothing</b>	6	6	4	6

RCA-SOFT and R-RCA-SOFT significantly outperform mRank and gRank, the latter two methods based on the percentage of broken edges are more sensitive to the anomaly prorogation.

Table IX. Top anomalies on coal plant data.

mRank	gRank	LBP	RCA	RCA-SOFT	R-RCA	R-RCA-SOFT
Y0039	Y0256	Y0256	X0146	X0146	X0146	X0146
X0128	Y0045	X0146	Y0045	Y0256	X0128	X0166
Y0256	Y0028	F0454	X0128	F0454	F0454	X0144
H0021	X0146	X0128	Y0030	J0079	Y0256	X0165
X0146	X0057	Y0039	X0057	Y0308	Y0039	X0142
X0149	X0061	X0166	X0158	X0166	Y0246	J0079
H0022	X0068	X0144	X0068	X0144	Y0045	X0164
F0454	X0143	X0149	X0061	X0128	Y0028	X0145
H0020	X0158	J0085	X0139	X0165	X0056	X0143
X0184	X0164	X0061	X0143	X0142	J0079	X0163
X0166	J0164	Y0030	H0021	H0022	X0149	J0164
J0164	H0021	J0079	F0454	X0143	X0145	X0149

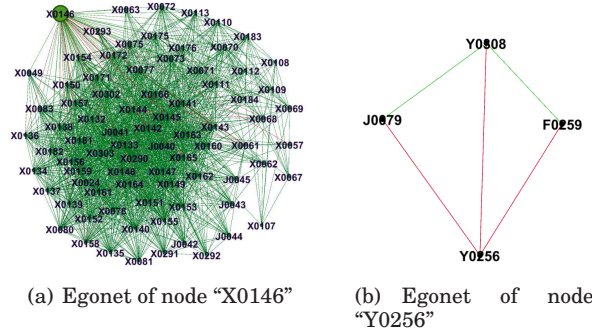


Fig. 8. Egonet of node "X0146" and "Y0256" in invariant network and vanishing correlations (red edges) on coal plant data.

We further validate the effectiveness of proposed methods with temporal smoothing. We report the top-12 results of different methods with smoothing at two successive time points  $t = 120$  and  $t = 121$  in Table VII. The number of "DB16"-related monitors in the top-12 results is summarized in Table VIII. From Tables VII and VIII, we observe a significant performance improvement of our methods with temporal broken networks smoothing compared with those without smoothing. As discussed in Sec. 6, since causal anomalies of a system usually do not change within a short period of time, utilizing such smoothness can effectively suppress noise and thus give better ranking accuracy.

### 8.3. Fault Diagnosis on Coal Plant Data

In this section, we test the proposed methods in the application of fault diagnosis on a coal plant cyber-physical system data. The data set contains time series collected through 1625 electric sensors installed on different components of the coal plant system. Using the invariant model described in Sec. 2.1, we generate the invariant network that contains 9451 invariant links. For privacy reasons, we remove sensitive descriptions of the data.

Based on knowledge from domain experts, in the abnormal stage the root cause is associated with component "X0146". We report the top-12 results of different ranking algorithms in Table IX. We observe that the proposed algorithms all rank component "X0146" the highest, while the baseline methods could give higher ranks to other components. In Fig. 8(a), we visualize the egonet of the node "X0146" in the invariant network, which is defined as the 1-step neighborhood around node "X0146", including the node itself, direct neighbors, and all connections among these nodes in the invariant network. Here, green lines denote the invariant link, and red lines denote vanishing correlations (broken links). Since the node "Y0256" is top-ranked by the baseline methods, we also visualize its egonet in Fig. 8(b) for a comparison. There are 80 links

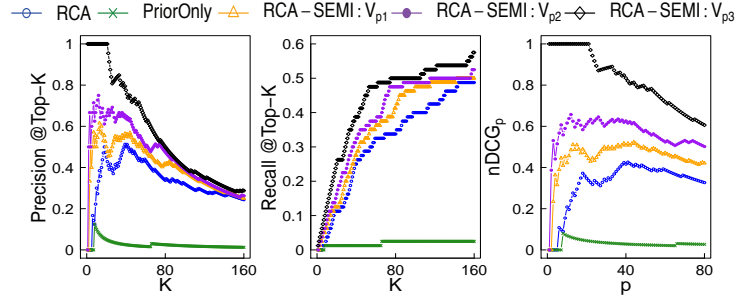


Fig. 9. Comparison on BIS data using prior knowledge. RCA-SEMI:V<sub>p1</sub>, RCA-SEMI:V<sub>p2</sub> and RCA-SEMI:V<sub>p3</sub> refer to running RCA-SEMI with  $\mathcal{V}_{p1}$ ,  $\mathcal{V}_{p2}$  and  $\mathcal{V}_{p3}$ , respectively.

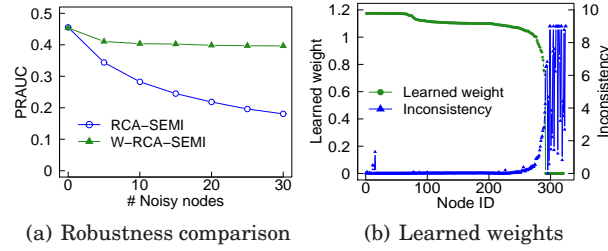


Fig. 10. Comparison on BIS data with noisy prior knowledge

related to “X0146” in the invariant network, and 14 of them are broken. Namely the percentage of broken edges is only 17.5% for a truly anomalous component. In contrast, the percentage of broken edges for the node “Y0256” is 100%, namely a false-positive node can have a very high percentage of broken edges in practice. This explains why baseline approaches using the percentage of broken edges could fail, because the percentage of broken edges does not serve as a reliable evidence of the degree of causal anomalies. In comparison, our approach takes into account the global structures of the invariant network via network propagation, thus the resultant ranking is more meaningful.

#### 8.4. Evaluation of Leveraging Prior Knowledge

In this section, we evaluate the effectiveness of the semi-supervised algorithms proposed in Sec. 7, using the BIS dataset. We simulate node attributes by the following strategy. First, we set “DB16” related components as seeds (recall these components are ground truth anomalies), and run label propagation algorithm to obtain a score for each node. Then, we set the scores of “DB16” related nodes to zero and treat the remaining non-zeros scores as the attributes of other nodes. Finally, we randomly divide the remaining attributed nodes  $\mathcal{V}_p$  into three equal parts  $\mathcal{V}_1$ ,  $\mathcal{V}_2$  and  $\mathcal{V}_3$ , and then form  $\mathcal{V}_{p1} = \mathcal{V}_1$ ,  $\mathcal{V}_{p2} = \{\mathcal{V}_1, \mathcal{V}_2\}$  and  $\mathcal{V}_{p3} = \{\mathcal{V}_1, \mathcal{V}_2, \mathcal{V}_3\}$ . Algorithm RCA-SEMI is run with  $\mathcal{V}_{p1}$ ,  $\mathcal{V}_{p2}$  and  $\mathcal{V}_{p3}$  respectively to evaluate its capability to uncover “DB16” related components with the guidance of these different partial prior knowledges.

Fig. 9 shows the results of RCA-SEMI. For clarity, we only show RCA as a baseline. We also consider another degraded version of RCA-SEMI, which is shown as “PriorOnly”. This method solves  $\mathbf{e}$  by minimizing  $(\mathbf{B}\mathbf{e} - \mathbf{v})^\top \mathbf{D}_u (\mathbf{B}\mathbf{e} - \mathbf{v}) + \tau \|\mathbf{e}\|_1$ , which only uses node attributes without considering label propagation. From Fig. 9, we observe RCA-SEMI can effectively incorporate node attributes to improve causal anomaly inference accuracy. More prior knowledge typically results in better accuracy. The poor

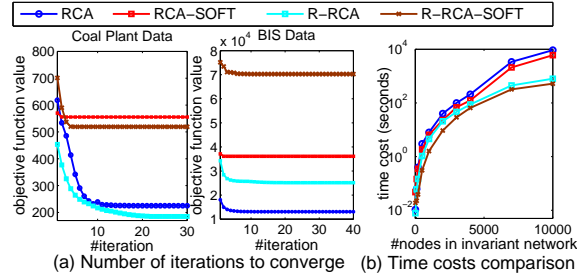


Fig. 11. Number of iterations to converge and time cost comparison.

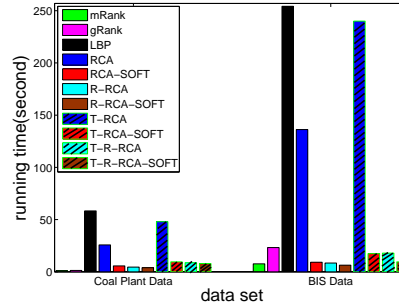


Fig. 12. Running time on real data sets.

performance of “PriorOnly” also indicates that using partial prior knowledge alone is not effective. This demonstrates the importance to take into account the fault propagation when incorporating partial node attributes.

Next, we evaluate the robustness of Alg. 2, W-RCA-SEMI. To this purpose, we manually inject noises in node attributes. Specifically, we randomly pick certain number of nodes with non-zero attributes, and change their attributes to a large value (e.g., 3). By varying the number of noisy nodes, we can evaluate the impacts of noises on RCA-SEMI and W-RCA-SEMI. Fig. 10(a) shows the area under the precision-recall curve (PRAUC) w.r.t. varying number of noisy nodes. Higher PRAUC indicates better accuracy. From Fig. 10(a), we observe the performance RCA-SEMI is largely impacted by the injected noisy attributes, while W-RCA-SEMI performs stably. By investigating the learned weights in  $u$ , we get the insights of W-RCA-SEMI. Fig. 10(b) presents the learned weights  $u_i$  vs. the inconsistency of  $(e_i - v_i)^2$  for nodes having valid  $v_i$ 's, where the nodes are ordered by descending order of  $u_i$ . As can be seen, W-RCA-SEMI effectively assigns small weights to large inconsistencies. Thus it can reduce the negative impacts of noisy attributes and obtain robust performance as shown in Fig. 10(a).

### 8.5. Time Performance Evaluation

In this section, we study the efficiency of proposed methods using the following metrics: 1) the number of iterations for convergence; 2) the running time (in seconds); and 3) the scalability of the proposed algorithms. Fig. 11(a) shows the value of the objective function with respect to the number of iterations on different data sets. We can observe that, the objective value decreases steadily with the number of iterations. Typically less than 100 iterations are needed for convergence. We also observe that our method with *softmax* normalization takes fewer iterations to converge. This is because the normalization is able to reduce the influence of extreme values [Sutton and Barto

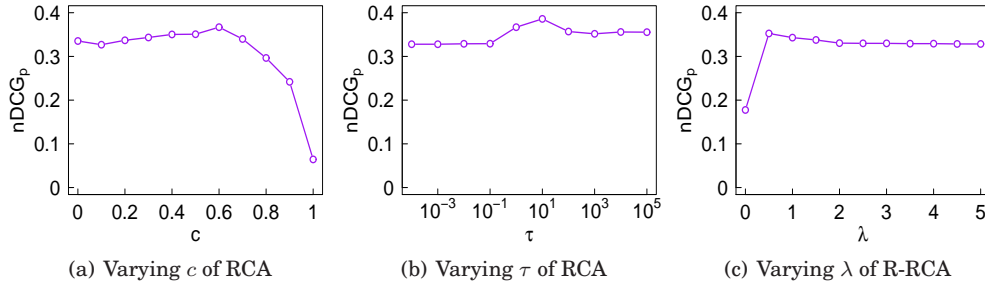


Fig. 13. Parameter study results. The shown nDCG values are obtained by varying one parameter while fixing others.

1998]. We also report the running time of each algorithm on the two real data sets in Fig. 12. We can see that the proposed methods can detect causal anomalies very efficiently, even with the temporal smoothing module.

To evaluate the computational scalability, we randomly generate invariant networks with different number of nodes (with network density=10) and examine the computational cost. Here 10% edges are randomly selected as broken links. Using simulated data, we compare the running time of RCA, R-RCA, RCA-SOFT, and R-RCA-SOFT. Fig. 11(b) plots the running time of different algorithms w.r.t. the number of nodes in the invariant network. We can see that the relaxed versions of our algorithm are computationally more efficient than the original RCA and RCA-SOFT. These results are consistent with the complexity analysis in Sec. 4.

### 8.6. Parameter Study

There are three major parameters  $c$ ,  $\tau$  and  $\lambda$  in the proposed RCA family algorithms.  $c$  is the trade-off parameter controlling the propagation strength (see Sec. 3.1).  $\tau$  is a parameter controlling the sparsity of the learned vector  $\mathbf{e}$  in Eq.(8).  $\lambda$  is used for balancing the propagation and broken network reconstruction in the relaxed RCA model in Eq. (23). Next, we use the BIS dataset to study the impact of each parameter on the causal anomaly ranking accuracy.

Fig. 13 shows the anomaly inference accuracy by varying each parameter in turn while fixing others. The accuracy is measured using nDCG<sub>p</sub> with  $p$  equal to the number of ground truth anomalies. Using other metrics will give similar trends thus are omitted for brevity. From the figure, we observe RCA and R-RCA perform stably in a relatively wide range of each parameter, which demonstrates the robustness of the proposed models. Specifically, the best  $c$  lies around 0.6, indicating the importance to consider sufficient fault propagations. Note when  $c = 0$  or  $c = 1$ , there will be no propagation or no learning of  $\mathbf{e}$  respectively (see Eq. (6)). For  $\tau$ , its best value is around 1 and 10, which suggests a sparse vector  $\mathbf{e}$  because usually there is only a small number of causal anomalies. Finally, the sharp accuracy increase by changing  $\lambda$  from 0 to non-zero values indicates the effectiveness of the relaxed RCA model in Eq. (23). The best  $\lambda$  lies between 0.5 and 2, suggesting the relatively equal importances of fault propagation and broken network reconstruction in Eq. (23).

## 9. RELATED WORK

In this section, we review related work on anomaly detection and system diagnosis, in particular along the following two categories: 1) fault detection in distributed systems; and 2) graph-based methods.



For the first category, Yemini et al. [Yemini et al. 1996] proposed to model event correlation and locate system faults using known dependency relationships between faults and symptoms. In real applications, however, it is usually hard to obtain such relationships precisely. To alleviate this limitation, Jiang et al. [Jiang et al. 2006a] developed several model-based approaches to detect the faults in complex distributed systems. They further proposed several Jaccard Coefficient based approaches to locate the faulty components [Jiang et al. 2006b; 2007]. These approaches generally focus on locating the faulty components, they are not capable of spotting or ranking the causal anomalies.

Recently, graph-based methods have drawn a lot of interest in system anomaly detections [Akoglu et al. 2015; Chandola et al. 2009], either in static graphs or dynamic graphs [Akoglu et al. 2015]. In static graphs, the main task is to spot anomalous network entities (e.g., nodes, edges, subgraphs) given the graph structure [Breunig et al. 2000; Henderson et al. 2010]. For example, Akoglu et al. [Akoglu et al. 2010] proposed the OddBall algorithm to detect anomalous nodes in weighted graphs. Liu et al. [Liu et al. 2005] proposed to use frequent subgraph mining to detect non-crashing bugs in software flow graphs. However, these approaches only focus on a single graph; in comparison, we take into account both the invariant graph and the broken correlations, which provides a more dynamic and complete picture for anomaly ranking. On dynamic graphs, anomaly detection aims at detecting abnormal events [Rossi et al. 2013]. Most approaches along this direction are designed to detect anomaly time-stamps in which suspicious events take place, but not to perform ranking on a large number of system components. Sun et al. proposed to use temporal graphs for anomaly detection [Sun et al. 2006]. In their approach, a set of initial suspects need to be provided; then internal relationship among these initial suspects is characterized for better understanding of the root cause of these anomalies.

In using the invariant graph and the broken invariance graph for anomaly detection, Jiang et al. [Jiang et al. 2006b] used the ratio of broken edges in the invariant network as the anomaly score for ranking; Ge et al. [Ge et al. 2014] proposed mRank and gRank to rank causal anomalies; Tao et al. [Tao et al. 2014] used the loopy belief propagation method to rank anomalies. As has been discussed, these algorithms rely heavily on the percentage of broken edges in egonet of a node. Such local approaches do not take into account the global network structures, neither the global fault propagation spreading on the network. Therefore the resultant rankings can be sub-optimal.

There is a number of correlation network based system anomaly localization methods [Idé et al. 2007; Idé et al. 2009; Hara et al. 2015], which treat the correlation changes between system components as the basic evidences of fault occurrences. Similar to the invariant graph based methods, these methods use the correlation changes in the egonet of each node at different time points to locate anomalous nodes. Basically, if there are more correlation changes happen in the egonet of a node, it is more suspicious to be an anomaly. However, none of these approaches consider fault propagations. Therefore, they cannot exploit the whole structure of a network and are inferior in locating causal anomalies. Some other methods can track the eigenvectors of temporal correlation networks to detect the anomalous changes of a whole system [Idé and Kashima 2004; Hirose et al. 2009], but they do not rank nodes for locating causal anomalies and are different from our work in problem settings.

## 10. CONCLUSIONS

Detecting causal anomalies on monitoring data of distributed systems is an important problem in data mining research. Robust and scalable approaches that can model the potential fault propagation are highly desirable. We develop a network diffusion based framework, which simultaneously takes into account fault propagation on the

network as well as reconstructing anomaly signatures using propagated anomalies. Our approach can locate causal anomalies more accurately than existing approaches; in the meantime, it is robust to noise and computationally efficient. Moreover, when prior knowledges on anomalous status of nodes are available, our approach can effectively incorporate them to further enhance anomaly detection accuracy. When the prior knowledges are noisy, our approach can also automatically identify reliable information and reduce negative impacts of noises. Using both synthetic and real-life data sets, we show that the proposed methods outperform other competitors by a large margin.

## REFERENCES

- Leman Akoglu, Mary McGlohon, and Christos Faloutsos. 2010. Oddball: Spotting anomalies in weighted graphs. In *PAKDD*. Springer, 410–421.
- Leman Akoglu, Hanghang Tong, and Danai Koutra. 2015. Graph based anomaly detection and description: a survey. *Data Min. Knowl. Discov.* 29, 3 (2015), 626–688.
- Stephen Boyd and Lieven Vandenberghe. 2004. *Convex optimization*. Cambridge university press.
- Markus M Breunig, Hans-Peter Kriegel, Raymond T Ng, and Jörg Sander. 2000. LOF: identifying density-based local outliers. In *SIGMOD*. ACM, 93–104.
- Varun Chandola, Arindam Banerjee, and Vipin Kumar. 2009. Anomaly detection: A survey. *ACM computing surveys* 41, 3 (2009), 15.
- Haifeng Chen, Haibin Cheng, Guofei Jiang, and Kenji Yoshihira. 2008. Exploiting local and global invariants for the management of large scale information systems. In *ICDM*. IEEE, 113–122.
- Yong Ge, Guofei Jiang, Min Ding, and Hui Xiong. 2014. Ranking metric anomaly in invariant networks. *ACM Trans. Knowl. Discov. Data* 8, 2 (2014), 8.
- Janos Gertler. 1998. *Fault detection and diagnosis in engineering systems*. CRC press.
- Satoshi Hara, Tetsuro Morimura, Toshihiro Takahashi, Hiroki Yanagisawa, and Taiji Suzuki. 2015. A consistent method for graph based anomaly localization. In *AISTATS*. 333–341.
- Keith Henderson, Tina Eliassi-Rad, Christos Faloutsos, Leman Akoglu, Lei Li, Koji Maruhashi, B Aditya Prakash, and Hanghang Tong. 2010. Metric forensics: a multi-level approach for mining volatile graphs. In *KDD*. ACM, 163–172.
- Shunsuke Hirose, Kenji Yamanishi, Takayuki Nakata, and Ryohei Fujimaki. 2009. Network anomaly detection based on eigen equation compression. In *KDD*. ACM, 1185–1194.
- Tsuyoshi Idé and Hisashi Kashima. 2004. Eigenspace-based anomaly detection in computer systems. In *KDD*. ACM, 440–449.
- Tsuyoshi Idé, Aurelie C Lozano, Naoki Abe, and Yan Liu. 2009. Proximity-based anomaly detection using sparse structure learning. In *SDM*. SIAM, 97–108.
- Tsuyoshi Idé, Spiros Papadimitriou, and Michail Vlachos. 2007. Computing correlation anomaly scores using stochastic nearest neighbors. In *ICDM*. IEEE, 523–528.
- Kalervo Järvelin and Jaana Kekäläinen. 2002. Cumulated gain-based evaluation of IR techniques. *ACM Trans. Inf. Syst.* 20, 4 (2002), 422–446.
- Guofei Jiang, Haifeng Chen, and Kenji Yoshihira. 2006a. Discovering likely invariants of distributed transaction systems for autonomic system management. In *ICAC*. IEEE, 199–208.
- Guofei Jiang, Haifeng Chen, and Kenji Yoshihira. 2006b. Modeling and tracking of transaction flow dynamics for fault detection in complex systems. *IEEE Trans. Dependable Secure Comput.* 3, 4 (2006), 312–326.
- Guofei Jiang, Haifeng Chen, and Kenji Yoshihira. 2007. Efficient and scalable algorithms for inferring likely invariants in distributed systems. *IEEE Trans. Knowl. Data Eng.* 19, 11 (2007), 1508–1523.
- Tae Hoon Kim, Kyoung Mu Lee, and Sang Uk Lee. 2008. Generative image segmentation using random walks with restart. In *ECCV*. Springer, 264–275.
- Daniel D Lee and H Sebastian Seung. 2001. Algorithms for non-negative matrix factorization. In *NIPS*. 556–562.
- Ljung Lennart. 1999. System identification: theory for the user. *PTR Prentice Hall, Upper Saddle River, NJ* (1999), 1–14.
- Chao Liu, Xifeng Yan, Hwanjo Yu, Jiawei Han, and S Yu Philip. 2005. Mining Behavior Graphs for “Back-trace” of Noncrashing Bugs.. In *SDM*. SIAM, 286–297.

- Ryan A Rossi, Brian Gallagher, Jennifer Neville, and Keith Henderson. 2013. Modeling dynamic behavior in large evolving graphs. In *WSDM*. ACM, 667–676.
- Jimeng Sun, Dacheng Tao, and Christos Faloutsos. 2006. Beyond streams and graphs: dynamic tensor analysis. In *KDD*. ACM, 374–383.
- Richard S Sutton and Andrew G Barto. 1998. *Reinforcement learning: An introduction*. MIT press Cambridge.
- Changxia Tao, Yong Ge, Qinbao Song, Yuan Ge, and Olufemi A Omitaomu. 2014. Metric Ranking of Invariant Networks with Belief Propagation. In *ICDM*. IEEE, 1001–1006.
- Robert Tibshirani. 1996. Regression shrinkage and selection via the lasso. *Journal of the Royal Statistical Society. Series B (Methodological)* (1996), 267–288.
- Hanghang Tong, Christos Faloutsos, and Jia-yu Pan. 2006. Fast Random Walk with Restart and Its Applications. In *ICDM*. IEEE, 613–622.
- Shaula Alexander Yemini, Shmuel Kliger, Eyal Mozes, Yechiam Yemini, and David Ohsie. 1996. High speed and robust event correlation. *IEEE communications magazine* 34, 5 (1996), 82–90.
- Guoxian Yu, Huzefa Rangwala, Carlotta Domeniconi, Guoji Zhang, and Zili Zhang. 2013. Protein function prediction by integrating multiple kernels. In *IJCAI*. AAAI Press, 1869–1875.
- Dengyong Zhou, Olivier Bousquet, Thomas Navin Lal, Jason Weston, and Bernhard Schölkopf. 2004. Learning with local and global consistency. In *NIPS*. 321–328.

Received February 2007; revised March 2009; accepted June 2009